A unified theory of aerodynamic and condensation shock waves in vapor-droplet flows with or without a carrier gas

Abhijit Guha
Whittle Laboratory, University of Cambridge, Madingley Road, Cambridge CB3 0DY, England

A unified theory for aerodynamic and condensation shock waves in vapor-droplet flows in the presence of an inert carrier gas is presented. Same conservation equations apply across discontinuous models for both types of wave. Exact (as well as approximate), explicit analytical jump conditions across such discontinuities are derived subject to several boundary conditions. Collectively they may be called the generalized Rankine–Hugoniot equations for vapor-droplet mixtures. All the equations derived are general and can be applied in the case of a pure vapor-droplet flow by letting the mass fraction of the carrier gas go to zero. Much physical insight may be obtained from this integral analysis. It is shown that four types of aerodynamic shock waves (viz., equilibrium partly dispersed, equilibrium fully dispersed, partly dispersed with complete evaporation, and fully dispersed with complete evaporation) may occur. Conditions for each type of these waves to occur are specified and the appropriate jump conditions are derived. A flow map for different types of condensation discontinuities to occur is deduced. It is shown that the same jump conditions are applicable for most supersonic and subsonic condensations—both homogeneous and heterogeneous. However, for certain types of condensation shocks predicted by the integral jump conditions, consideration of nonequilibrium gas dynamics must be called for. As a sequel to the integral analysis, time-marching solutions for different types of condensation shock waves in a convergent–divergent nozzle are presented, which include some novel solutions. Isentropic exponents for gas–vapor-droplet flow under frozen and equilibrium conditions are formulated. Gasdynamic equations for vapor-droplet flow, including area variation and interphase transport of mass, momentum, and energy, are derived. It is shown that equations in this full form are to be considered for making correct physical interpretations, e.g., determining the conditions for thermal choking.

I. INTRODUCTION

The thermofluid dynamics of the two-phase flow of a vapor-droplet mixture consisting of a large number of minute liquid droplets uniformly dispersed throughout a background vapor phase continuum is both scientifically interesting and of engineering importance (in a variety of areas of mechanical engineering, chemical engineering, and meteorology). Applications include condensing flows of moist air or combustion products, aerosol formation in mixing processes, aerodynamic testing in cryogenic wind tunnels, and wetness problems in large, low-pressure steam turbines used for electricity generation. In this article, we present a unified, control-volume analysis for different types of discontinuities (similar to the analysis of an adiabatic shock wave in an ideal gas) that occur in vapor-droplet mixtures under a variety of operating conditions. (Note, however, that although they can be modeled as mathematical discontinuities for many practical purposes and many useful aspects can be studied from such models, no actual, physical discontinuities are involved. Physical mechanisms such as viscous dissipation, thermal conduction, and relaxation give rise to a continuous variation of flow properties, even if over a small length scale.) The integral treatment is then complemented by analysis and numerical solutions of the differential equations of motion.

One application of the integral, discontinuous model is involved with the formation of the liquid droplets itself.

When a dry mixture of an inert gas and a condensable vapor is expanded rapidly, liquid droplets do not form as soon as the vapor reaches the saturation temperature. The vapor goes out of equilibrium and attains considerable subcooling (i.e., the vapor temperature falls below the local saturation value) due to continued expansion. The rate of formation of liquid nuclei is very strongly dependent on the subcooling. Thus when the subcooling becomes appreciable, a very large number of very small nuclei form over a relatively short time. These nuclei grow by exchanging heat and mass with the surrounding, subcooled vapor. The resulting release of latent heat is conducted back to the vapor and the vapor temperature quickly rises to the local saturation value (i.e., the subcooling decreases to almost zero). This rapid reversion to equilibrium is generally termed condensation shock and has been the topic of an extremely large number of studies.[1-11] (The term condensation shock is, in general, a misnomer. Although heat addition in a supersonic flow results in an increase in pressure, the rise is gradual and the Mach number at the end of the condensation zone, in general, remains above unity.)

On the other hand, aerodynamic shock waves may form in a supersonic, two-phase, vapor-droplet flow in the same way as they form in an ideal gas. However, the analysis is more complicated than that in an ideal gas because there is no unique sonic speed in a vapor-droplet mixture, and nonequilibrium exchanges of mass, momentum, and energy between the two phases are involved. The general
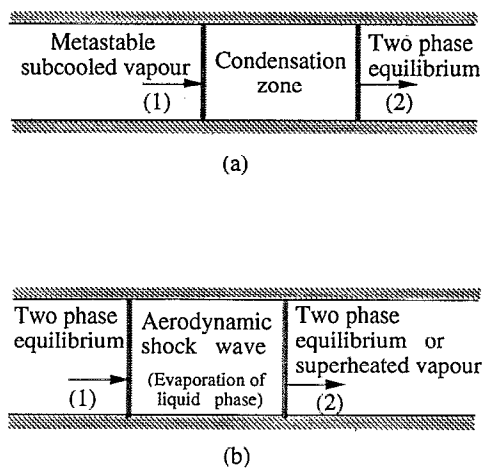
FIG. 1. Control volume analysis of discontinuities: (a) condensation shock, (b) aerodynamic shock wave.

behavior of condensing flow and the propagation of small-amplitude harmonic waves in vapor-droplet mixtures have been studied extensively.[12,13] Although the structure of shock waves in a general relaxing medium has been discussed in many publications[14,15] in the past, the work on shock waves in vapor-droplet mixtures is rather recent.[16–23] A practical example of two-phase aerodynamic shock waves occurs near blade trailing edges in the last, transonic stages of low-pressure steam turbines used in power plants.

In this article, we perform a Rankine–Hugoniot-type analysis describing the jump conditions across aerodynamic as well as condensation shock waves. Approximate as well as exact, explicit jump conditions have been derived (which have not been considered in the literature previously). The same conservation equations hold for both types of discontinuities but lead to different solutions depending on the boundary conditions. It is therefore instructive to study both types of discontinuities from a common standpoint. Figure 1 schematically depicts the control-volume models applied in the present study.

Note that the fluid is at a metastable, subcooled state upstream of a condensation shock wave but is at two-phase equilibrium downstream of it. On the other hand, the fluid is at two-phase equilibrium upstream of an aerodynamic shock wave but may be either superheated or at two-phase equilibrium downstream. Moreover, *evaporation* of liquid droplets takes place across an aerodynamic shock wave, whereas *condensation* takes place in a condensation discontinuity. Thus phase change effectively results in *heat removal* for the vapor phase in the former case, and in *heat addition* in the latter. The entropy of the medium, however, increases across both types of discontinuities, as is dictated by the second law of thermodynamics. This has important implications on permissible upstream and downstream Mach numbers in the two cases.

Another subtle difference between the two cases arises because it may be normally assumed that individual droplet radii change solely due to pure evaporation or condensation. Coagulation of droplets is neglected and the Weber number criterion for stability against fragmentation is well satisfied even for very strong shock wave deceleration.[19] Each droplet, therefore, retains its individual identity and the number of droplets per unit mass does not change across an aerodynamic shock wave (unless a droplet is evaporated completely). On the other hand, new liquid droplets obviously nucleate before their rapid growth results in a condensation shock wave. Integral conservation equations, either across an aerodynamic or a condensation shock, however, depend on the total moisture content and not on its distribution among different droplet size groups.

For the sake of generality, we assume that the vapor phase consists of a condensable vapor and an inert, carrier gas. However, the formulas derived and the conclusions deduced are equally applicable to pure vapor-droplet flows. For example, the jump conditions across aerodynamic shock waves in pure vapor-droplet flows (given in Ref. 16) can be recovered from the jump conditions across aerodynamic shock waves given here simply be letting the mass fraction of the carrier gas go to zero.

II. MODELING THE MIXTURE

Consider a gas–liquid droplet mixture. The gas phase is the continuous phase and, in general, consists of a mixture of an inert gas and a condensable vapor. The liquid phase is the discontinuous phase and consists of a polydispersed population of spherical droplets of the same chemical species as the condensable vapor. The inert gas, vapor, and liquid droplets are referred to by subscripts g, v, and l, respectively.

If the mass fraction of the inert gas per unit mass of the mixture is denoted by g, the mass of vapor plus liquid per unit mass of mixture is $(1-g)$. The wetness fraction y is then defined as the mass of liquid per unit mass of vapor plus liquid. Therefore, the mass of vapor per unit mass of mixture is $(1-g)(1-y)$ and the total mass of liquid per unit mass of mixture is $(1-g)y$.

The above definitions of g and y are very convenient. In the absence of velocity slip between the gas and liquid phases, elemental fluid particles retain their identity in that the total mass of vapor plus liquid contained in the particle remains constant even though condensation or evaporation may occur. Under these conditions, it follows that g remains constant along a particle path line in unsteady flow or along a streamline in steady flow. Furthermore, any generalized set of equations can be converted to the special case by letting the appropriate quantity go to its limiting value. For example, for a pure vapor $g=0$, and y is synonymous with the conventional definition of the wetness fraction. The condition $g=1$ renders the medium to consist of the inert gas only, and $y=0$ renders the medium to be a mixture of the inert gas and superheated vapor. In passing, note that the specific humidity (defined for mixtures of low vapor content as the ratio of the mass of vapor to the mass of inert gas) is given by $(1-g)(1-y)/g$.

If ρ is the density of the gas phase (inert gas+vapor) and ρ_l is the material density of the liquid phase, then the mixture density ρ_m is calculated from

$$\frac{1}{\rho_m} = \frac{g + (1-g)(1-y)}{\rho} + \frac{(1-g)y}{\rho_l}. \tag{1}$$

However, usually $\rho_l \gg \rho$. The usually small numerator of the second term in the right-hand side (RHS) of Eq. (1) makes its contribution to the total density even less significant and hence the second term can be neglected for most practical calculations.

The inert gas and the vapor are assumed to behave as perfect gases with partial pressures p_g and p_v, respectively.

$$p_g = \rho_g R_g T, \tag{2}$$

$$p_v = \rho_v R_v T, \tag{3}$$

where ρ_g and ρ_v are the *partial* densities and R_g, R_v are the specific gas constants for the inert gas and vapor, respectively, and T is the common temperature of the gas phase. By Dalton's law the partial pressures and densities are additive:

$$p = p_g + p_v, \tag{4}$$

$$\rho = \rho_g + \rho_v, \tag{5}$$

where p is the mixture pressure. Equation (4) implies that the partial pressure due to the liquid droplets is negligible. Note the difference in combining component densities in Eqs. (1) and (5). In Eq. (1), ρ_l is the actual material density of the liquid phase. Hence specific volumes, rather than density, of the individual phases are added to calculate the mixture specific volume. From Eqs. (1)–(5)

$$p = \rho RT = \rho_m \bar{R} T, \tag{6}$$

where

$$R = \frac{g R_g + (1-g)(1-y) R_v}{g + (1-g)(1-y)} \tag{7}$$

and

$$\bar{R} = g R_g + (1-g)(1-y) R_v. \tag{8}$$

Both R and $\bar{R}$ may vary from point to point in the flow field. The specific enthalpy of the gas–vapor-droplet mixture, $\bar{h}$, comprises of the contribution from individual components and is given by

$$\bar{h} = g h_g + (1-g)(1-y) h_v + (1-g) y h_l. \tag{9}$$

Equation (9) is a general expression valid under nonequilibrium conditions as well, in which case h_l would be calculated at the liquid phase temperature (different from gas phase temperature) and also y would not be the equilibrium wetness fraction.

The partial pressure p_v is related to the mixture pressure p through Eqs. (2)–(8), which can be simplified to

$$\frac{p_v}{p} = \frac{(1-g)(1-y) R_v}{g R_g + (1-g)(1-y) R_v}. \tag{10}$$

III. DETERMINATION OF ISENTROPIC EXPONENTS OF THE MIXTURE

The gas–vapor-droplet mixture is a relaxing medium and, following relaxation gas dynamics,[24] there can be two limiting types of flow in which the entropy of the mixture remains constant. Many different expressions for the isentropic exponent in the two limiting cases can be found in the literature.[3,9,11,25] We, therefore, include a short derivation of the correct form of the exponents.

A. Frozen flow

This case arises when interphase transport of mass, momentum, and energy between the gas phase and the liquid droplets are frozen completely. In other words, the liquid droplets do not take part in the fluid mechanical processes. It can be shown that the thermodynamic form of the energy equation in this case is given by

$$\frac{g}{g + (1-g)(1-y)} dh_g + \frac{(1-g)(1-y)}{g + (1-g)(1-y)} dh_v = \frac{dp}{\rho}, \tag{11}$$

where ρ is the gas phase density and the left-hand side (LHS) of (11) is the mass-fraction-weighted sum of the changes in specific enthalpies of the inert gas and the condensable vapor (without the liquid droplets). Invoking the ideal gas assumption, Eq. (11) can be rewritten as

$$\frac{dp}{\rho} = \frac{[g c_{pg} + (1-g)(1-y) c_{pv}]}{[g + (1-g)(1-y)]} dT \equiv c_p dT, \tag{12}$$

where c_{pg} and c_{pv} are the isobaric specific heat capacities of the inert gas and vapor, respectively, and T is their common temperature. Equations (6) and (12) can be combined to show that p / ρ^{γ_f} remains constant in an isentropic process, where the frozen exponent γ_f is given by

$$\gamma_f = \frac{g c_{pg} + (1-g)(1-y) c_{pv}}{g(c_{pg} - R_g) + (1-g)(1-y)(c_{pv} - R_v)}. \tag{13}$$

Accordingly, the frozen speed of sound, a_f, can be defined by

$$a_f = \sqrt{\gamma_f p / \rho} = \sqrt{\gamma_f RT}, \tag{14}$$

where R is given by (7). If the flow velocity is V, then a frozen Mach number may be defined as $M_f = V / a_f$.

The frozen exponent γ_f, given by Eq. (13), can be interpreted as usual as $\gamma_f = c_p / (c_p - R)$ where c_p and R are given by Eqs. (12) and (7), respectively. The relevant properties are weighted averages according to the composition of the gas phase only (*not the mixture*). It is important to note that the liquid phase does not take part in the dynamics of the flow process under the assumed conditions and the liquid flow properties do not change. But, with the present notations, different values of y for a fixed g changes the ratio of the mass fractions of the inert gas and the vapor. Hence the wetness fraction y appears in the expression for the frozen exponent γ_f in Eq. (13). In the limits $g=0$ and 1, γ_f given by Eq. (13) reduces to the isentropic exponents of the vapor phase, γ_v, and of the inert gas, γ_g, respectively.

The expressions for γ_f given in Refs. 9, 11, and 25 all tend to γ_g as $g \to 1$ (in accordance with the present theory). However, those expressions become increasingly more *inaccurate* as the mass fraction of the vapor increases, and *do not tend to γ_v as $g \to 0$* (the present theory does). According to the expressions of Refs. 9 and 25, as $g \to 0$, $\gamma_f \to \gamma_v(1-y)/[1+y(\gamma_v-1)]$; according to Ref. 11, as $g \to 0$, $\gamma_f \to [(1-y)c_{pv}+yc_l]/[(1-y)(c_{pv}-R_v)+yc_l]$, where c_l is the liquid specific heat. In pure steam–water mixture with $y = 0.1$, for example, the expressions of Refs. 9 and 25 would give $\gamma_f = 0.87\,\gamma_v$, and the expression of Ref. 11 would give $\gamma_f = 0.94\,\gamma_v$.

B. Equilibrium flow

When the liquid droplets are always in complete equilibrium with their own vapor, the laws of equilibrium thermodynamics hold good and any entropy production due to the relaxation mechanism vanishes. Conditions of equilibrium are that the velocity and temperature (neglecting surface effects for established droplet sizes) of the gas and liquid phases are equal and also that the partial pressure due to the vapor is equal to the saturation pressure corresponding to its temperature. Hence, the vapor pressure changes according to the Clausius–Clapeyron equation

$$\frac{dp_v}{p_v} = \frac{h_{fg}}{R_v T}\frac{dT}{T},\tag{15}$$

where h_{fg} is the specific enthalpy of evaporation which is a known function of temperature. Later we shall symbolically refer to this relation as $p_v = p_s(T)$. Equations (10) and (15) together show that for particular values of p, T, and g, the equilibrium wetness fraction y is *fixed*. Any arbitrary combination of p, T, and g may not satisfy the requirements of *two-phase equilibrium*. For example, p cannot be less than the saturation pressure at T. Also note that to maintain the equilibrium partial pressure there must be some vapor in the mixture. In other words, at equilibrium, y can never be equal to 1. On the other hand, a mixture of inert gas and superheated vapor (without any liquid) can be at equilibrium.

The thermodynamic relation for an isentropic process in the *equilibrium* gas–vapor-droplet mixture becomes

$$d\bar{h} = \frac{dp}{\rho_m}.\tag{16}$$

The value of $d\bar{h}$ is obtained by differentiating Eq. (9) under the assumption that all the components of the mixture are at temperature T

$$d\bar{h} = \bar{c}_p dT - (1-g)h_{fg}dy,\tag{17}$$

where

$$\bar{c}_p = gc_{pg} + (1-g)(1-y)c_{pv} + (1-g)yc_l.\tag{18}$$

For thermodynamic consistency, since the specific heats of the vapor c_{pv} and that of the liquid c_l are assumed to be constant, h_{fg} should vary with temperature such that

$$\frac{dh_{fg}}{dT} = c_{pv} - c_l.\tag{19}$$

Differentiating the equations of state (6) and (8), we obtain

$$\frac{dp}{p} = \frac{d\rho_m}{\rho_m} + \frac{d\bar{R}}{\bar{R}} + \frac{dT}{T} = \frac{d\rho_m}{\rho_m} - \frac{(1-g)R_v}{\bar{R}}dy + \frac{dT}{T}.\tag{20}$$

From Eqs. (10) and (15)

$$\frac{dp}{p} = \left(\frac{1}{1-y} - (1-g)\frac{R_v}{\bar{R}}\right)dy + \frac{h_{fg}}{R_v T}\frac{dT}{T}.\tag{21}$$

Eliminating dy between Eqs. (20) and (21) one obtains the relation between dp, $d\rho_m$, and dT as

$$\frac{dp}{p} = \frac{gR_g}{\bar{R}}\frac{d\rho_m}{\rho_m} + \left[1 + \frac{(1-g)(1-y)R_v}{\bar{R}}\left(\frac{h_{fg}}{R_v T} - 1\right)\right]\frac{dT}{T}.\tag{22}$$

Now, eliminating dT and dy from Eqs. (16), (17), (20), and (22) one obtains

$$\frac{dp}{p} = \gamma_e \frac{d\rho_m}{\rho_m},\tag{23}$$

where

$$\gamma_e = \frac{1 + (R_g/\bar{R})[g/(1-g)(1-y)](\bar{c}_p T/h_{fg})(R_v T/h_{fg})}{1 - 2(R_v T/h_{fg}) + [1/(1-g)(1-y)](R_v T/h_{fg})[(\bar{c}_p T/h_{fg}) - (gR_g T/h_{fg})]}.\tag{24}$$

Integration of Eq. (23) shows that $p/\rho_m^{\gamma_e}$ remains constant in an isentropic process (if the variation in γ_e is small). As an example, the values of γ_e in the air–water mixture for some specified conditions are plotted in Fig. 2. Interestingly, even for small mass fractions of H_2O, $(1-g)$, the values of γ_e in the air–water mixture is quite close to that in the *pure* water vapor-droplet mixture (given in Ref. 16).

The dotted line in Fig. 2 represents the maximum value of g for maintaining equilibrium at the specified pressure and temperature.

The expression of γ_e, given by Eq. (24), reduces to known expressions in the appropriate limits.

(i) In the case of pure vapor-droplet flow, $g \to 0$ and γ_e reduces to the familiar expression[16]
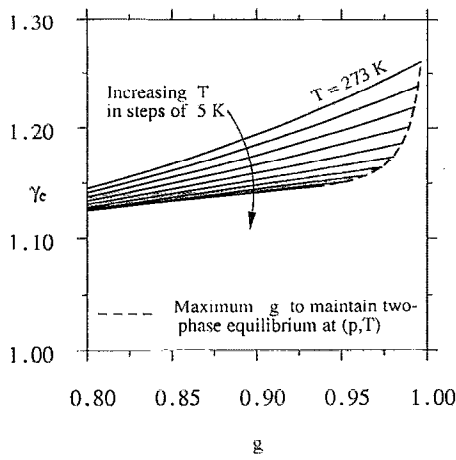
FIG. 2. Isentropic exponent in an equilibrium air–water mixture as a function of gas mass fraction ($p=1$ bar, varying T).

$$\gamma_e = \frac{1}{1 - 2(R_v T/h_{fg}) + (R_v T/h_{fg})(cT/h_{fg})}, \qquad (25)$$

where

$$c = c_{pv} + \frac{y}{1-y} c_l. \qquad (26)$$

(ii) In the case of pure gas, $g \to 1$, $y \to 0$, $\gamma_e \to \gamma_g$. (See Fig. 2.)

However, note that if $g \neq 1$ and $y \to 0$, then γ_e does not tend to the frozen value γ_f [Eq. (13)], as would be expected. The reason for such a discrepancy lies in the use of the Clausius–Clapeyron equation [Eq. (15)] while deriving Eq. (24), which does not remain valid in the absence of the liquid phase. The existence of a similar discontinuity in the value of the isentropic exponent in the case of pure vapor is noted in Ref. 19 and has been explained there.

The equilibrium sonic speed in gas–vapor-droplet mixture is simply given by

$$a_e = \sqrt{\gamma_e p / \rho_m} = \sqrt{\gamma_e \bar{R} T}, \qquad (27)$$

where $\bar{R}$ is given by Eq. (8). If the flow velocity is V then an equilibrium Mach number M_e may be defined such that $M_e = V/a_e$. The equilibrium speed of sound is always less than the frozen speed of sound in any relaxing medium $(a_f > a_e)$.[24] Therefore, it follows, that the local equilibrium Mach number at any point in the flow field is higher than the local frozen Mach number $(M_e > M_f)$.

It can be shown that the expression for γ_e in Ref. 11 is the same as Eq. (24). γ_e given in Ref. 25 is, however, not quite correct and does not reduce to Eq. (25) in the limit of pure vapor-droplet flow $(g \to 0)$. A detailed study shows that the discrepancy can be traced to the assumption of constant h_{fg} and to the use of $\tilde{c}_p$ [given by Eq. (31)] in Refs. 3 and 25 instead of $\bar{c}_p$ [given by Eq. (18)] in the energy Eq. (17).

IV. AERODYNAMIC SHOCK WAVES

A. Jump conditions across normal shock waves when the boundary conditions are equilibrium states

We now consider the structure of stationary, finite-amplitude waves in one-dimensional steady flow of a gas–vapor-droplet mixture. Far upstream of the wave (denoted by subscript 1) the flow is assumed to be in thermodynamic and inertial equilibrium with a prescribed pressure, temperature, and mass fraction g. Far downstream of the wave (denoted by subscript 2) a new two-phase equilibrium condition is re-established. The continuity, momentum, and energy equations for the two-phase mixture connecting the two end equilibrium states across a normal shock wave take the form

continuity $\quad \rho_{m1} V_1 = \rho_{m2} V_2$, $\qquad (28)$

momentum $\quad p_1 + \rho_{m1} V_1^2 = p_2 + \rho_{m2} V_2^2$, $\qquad (29)$

energy $\quad h_1 + \tfrac{1}{2} V_1^2 = h_2 + \tfrac{1}{2} V_2^2$. $\qquad (30)$

With the help of the definition

$$\tilde{c}_p = g c_{pg} + (1-g) c_{pv} \qquad (31)$$

and Eq. (9), Eq. (30) becomes

$$\tilde{c}_p T_1 - (1-g) y_1 h_{fg1} + V_1^2/2 = \tilde{c}_p T_2 - (1-g) y_2 h_{fg2} + V_2^2/2. \qquad (32)$$

Note that the same value of g applies to the far upstream and far downstream ends and $\tilde{c}_p$ remains constant. Equations (6), (10), and (15) are applicable to both ends of the shock wave as well. The equation set (6), (10), (15), (28), (29), and (32) therefore furnish altogether nine relations between thirteen variables and hence can be solved if any four of the variables are prescribed. However, no general analytical solution is possible if all four are specified at the upstream and the equations have to be solved by an iterative numerical scheme. For moderate strengths of shock waves, it is, however, possible to obtain an approximate analytical solution and this has been derived below. Later it is also shown that if instead of specifying the upstream velocity V_1, the temperature ratio across the shock is prescribed a completely general analytical solution of the above-mentioned equation set is possible.

1. Approximate Rankine–Hugoniot relations (for specified p_1, T_1, V_1, and g)

The ratio of the different flow variables between the two end states of a normal shock wave in an ideal gas can be expressed as functions of the upstream Mach number. They are generally referred to as the Rankine–Hugoniot relations. In the case of a simpler relaxing medium (e.g., solid-particle-laden gas), it can be shown that these relations remain identical[15] if the upstream equilibrium Mach number (M_{e1}) is used instead of the frozen Mach number (M_{f1}). These relations are exact and hold unconditionally. Derivation of similar relations in gas–vapor-droplet flow involves approximations and the derived relations are of conditional applicability. Difficulties arise mainly because of the mass transfer between the vapor and the liquid phase

and also because the partial pressure and temperature of the vapor at equilibrium with liquid droplets are not independent of each other but are connected via the Clausius–Clapeyron equation $[p_v = p_s(T)]$.

If the shock wave is weak so that the entropy change is small, we can write the thermodynamic relation for the two-phase mixture by combining Eqs. (16) and (23)

$$d\bar{h} = \frac{\gamma_e}{\gamma_e - 1} d\left(\frac{p}{\rho_m}\right). \tag{33}$$

Assuming γ_e does not change appreciably between end states, Eq. (33) may be integrated to give

$$\bar{h}_2 - \bar{h}_1 = \frac{\gamma_e}{\gamma_e - 1}\left(\frac{p_2}{\rho_{m2}} - \frac{p_1}{\rho_{m1}}\right). \tag{34}$$

Substitution of Eq. (34) in the energy equation (30) results in

$$\frac{\gamma_e}{\gamma_e - 1}\left(\frac{p_1}{\rho_{m1}}\right) + \frac{1}{2} V_1^2 = \frac{\gamma_e}{\gamma_e - 1}\left(\frac{p_2}{\rho_{m2}}\right) + \frac{1}{2} V_2^2. \tag{35}$$

Equation (35) is analogous to the energy equation for the adiabatic flow of a single-phase ideal gas. However, in the case of ideal gas, $dh_g = c_{pg} dT_g = \gamma_g/(\gamma_g - 1)d(p/\rho_g)$ is a general identity and hence the analog of Eq. (35) is generally valid for any arbitrary adiabatic process in an ideal gas. This may not be the case for gas–vapor-droplet flow. However, although Eq. (35) was derived subject to the assumptions of the isentropic process and constancy of γ_e, it applies reasonably well across shock waves of low to moderate strength. (This will be shown when calculations based on approximate Rankine–Hugoniot relations are later compared with an exact solution.) One of the conditions, as discussed in Sec. IV B, for using Eq. (35) is that complete evaporation of the liquid droplets does not occur and this restricts the upper limit of the upstream Mach number to rather low values.

Once the energy equation, Eq. (30), is replaced by Eq. (35), the resulting set of Eqs. (28), (29), and (35) are identical with the ideal gas analogs, and the Rankine–Hugoniot relations may be derived following the standard procedure given in any gasdynamics textbook. The results are

$$\frac{p_2}{p_1} = \frac{2\gamma_e}{\gamma_e + 1} M_{e1}^2 - \frac{\gamma_e - 1}{\gamma_e + 1}, \tag{36}$$

$$\frac{V_2}{V_1} = \frac{(\gamma_e - 1)M_{e1}^2 + 2}{(\gamma_e + 1)M_{e1}^2}, \tag{37}$$

$$\frac{\rho_{m2}}{\rho_{m1}} = \frac{V_1}{V_2}, \tag{38}$$

where the upstream equilibrium Mach number M_{e1} is given by

$$M_{e1} = \frac{V_1}{a_{e1}} = \frac{V_1}{(\gamma_e p_1/\rho_{m1})^{1/2}}. \tag{39}$$

The range of acceptability of the above equations depends on the validity of Eq. (35). [The accuracy of Eqs. (36)–
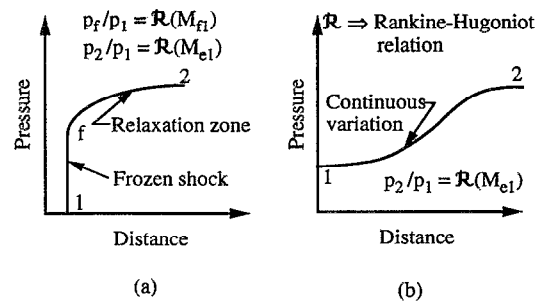

FIG. 3. Schematic structure of aerodynamic shock waves in a relaxing medium: (a) partly dispersed wave, $M_{e1} > 1$, $M_{f1} > 1$, (b) fully dispersed wave, $M_{e1} > 1$, $M_{f1} < 1$.

(38) is compared with an exact solution given later in Sec. IV A 2.] However, although not exact, these equations have two advantages: (i) all shock relations could be explicitly written in terms of the upstream parameters only, and (ii) the form of the equations is similar to the well-known Rankine–Hugoniot relations for ideal gas.

It should be noted that Eqs. (36)–(38) are valid for both partly and fully dispersed shock waves. Partly dispersed shock waves arise when the upstream frozen Mach number is greater than unity ($M_{f1} > 1$ also implies $M_{e1} > 1$). They are characterized by an almost discontinuous wave front, dominated by viscous dissipation and thermal conduction, followed by a continuous relaxation zone. The jump conditions across the discontinuous wave front (termed frozen shock) is given by the classical Rankine–Hugoniot relations *based on M_{f1}*. Equations (36)–(38), on the other hand give the overall changes in flow properties across the entire shock wave (frozen shock + relaxation zone). Fully dispersed waves do not involve any frozen discontinuity and give rise to continuous variation of flow properties from one equilibrium state to another. They may appear in the flow field if the upstream velocity is such that $M_{f1} < 1$, but $M_{e1} > 1$. Equations (36)–(38) specify the jump conditions across fully dispersed waves as well. This point is schematically presented in Fig. 3.

2. An exact solution (for specified p_1, T_1, T_2, and g)

If instead of specifying the upstream velocity V_1, the temperature ratio T_2/T_1 across the shock wave is treated as an independent variable, an exact solution of Eqs. (28), (29), and (32) can be formulated (without requiring any approximate energy equation such as that used in Sec. IV A 1).

The algebra is quite complicated but, briefly, the steps are as follows. The vapor pressure p_{v2} is known from Eq. (15). The mixture pressure p_2 in Eq. (29) is expressed in terms of p_{v2} and y_2 by Eq. (10). The downstream mixture density ρ_{m2} is expressed in terms of T_2, p_{v2} and y_2 by Eqs. (6) and (10). The downstream velocity V_2 in Eqs. (29) and (32) is then expressed in terms of V_1 by the continuity equation (28). V_1 is then eliminated from the resulting two equations to give a quadratic equation in y_2. The solution is
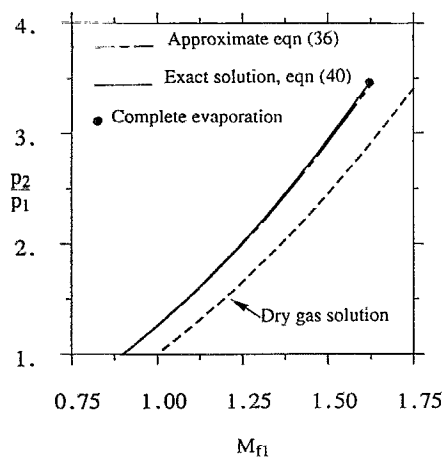
FIG. 4. Comparison of an approximate Rankine–Hugoniot solution with an exact jump condition for aerodynamic shock waves (air–water mixture, $p_1 = 1$ bar, $T = 293$ K, $g = 0.95$).

$$1 - y_2 = \frac{B + \sqrt{B^2 + 4AC}}{2A}, \tag{40}$$

where

$$A = 2(1-g)h_{fg2} - \frac{p_{v2} - p_1}{p_{v2}} T_2 (1-g)R_v,$$

$$B = 2(1-g)(h_{fg2} - y_1 h_{fg1}) + 2\widetilde{c}_p(T_1 - T_2) + gR_g T_2$$
$$+ \frac{p_{v2} - p_1}{\rho_{m1}},$$

$$C = \frac{gR_g}{(1-g)R_v} \frac{p_{v2}}{\rho_{m1}}.$$

The dimensions of A, B, and C in Eq. (40) are that of energy per unit mass. A and C are positive. Therefore the requirement that $0 < y_2 < 1$ eliminates the other root in Eq. (40). Equation (40) reduces to Eq. (29) of Ref. 16 in the special case of the pure vapor-droplet mixture ($g=0$, $C=0$).

Once y_2 is found, p_2 may be calculated from Eq. (10) and ρ_{m2} from Eq. (6). The flow velocities V_1 and V_2 may then be determined from Eqs. (28) and (29).

The pressure ratio p_2/p_1 calculated for an air–water mixture from this exact solution procedure is plotted as a function of the upstream frozen Mach number (V_1/a_{f1}) as the solid line in Fig. 4. Also included in the figure is the approximate relation, Eq. (36). It can be seen that the approximate relation performs quite well until the mixture is close to complete evaporation. The dotted line in the same figure gives the pressure ratio across shock waves in a *dry* mixture (with the same value of g as in the wet mixture). The rise in pressure in the wet mixture is more than that in the dry mixture because further increase in pressure takes place in the relaxation zone following the frozen shock. It is to be noted that steady shock waves exist in a wet mixture even for $M_{f1} < 1$. These waves are termed fully dispersed waves. Both Eqs. (36) and (40) apply across such waves.

B. Limiting wetness fraction

In the previous section it was assumed that downstream of the shock wave the medium is an equilibrium mixture of the gas phase and the liquid droplets. However, the liquid droplets *evaporate* in a fully dispersed wave or in the relaxation zone of a partly dispersed wave. Hence if the strength of the shock wave is substantial, the whole of the liquid phase may evaporate. This would render the medium at the downstream end as a single-phase mixture of the inert gas and superheated vapor. The vapor pressure is no longer restrained to the saturation pressure corresponding to the mixture temperature and none of the equations derived in Secs. IV A 1 and IV A 2 would be valid. Note, however, that the value of g does not change as a result of the complete evaporation of the liquid phase.

The limiting wetness fraction $y_{1,\text{lim}}$ can be determined by letting y_2 go to zero in Eq. (40). If the upstream wetness fraction is less than this limiting value corresponding to a shock of particular strength, complete evaporation takes place in the dispersed wave. Thus

$$y_{1,\text{lim}} = \left[\frac{T_2}{T_1}\left(\frac{p_{v2} - p_1}{p_{v2}} + \frac{gR_g - 2\widetilde{c}_p}{(1-g)R_v}\right) + \left(1 + \frac{g}{1-g}\frac{R_g}{R_v}\right)\right.$$
$$\times \left(\frac{p_{v2} - p_1}{p_1} + \frac{g}{1-g}\frac{R_g}{R_v}\frac{p_{v2}}{p_1}\right)$$
$$\left. + \frac{2\widetilde{c}_p}{(1-g)R_v}\right] \bigg/ \left(\frac{2h_{fg1}}{R_v T_1} + \frac{p_{v2} - p_1}{p_1} + \frac{g}{1-g}\frac{R_g}{R_v}\frac{p_{v2}}{p_1}\right); \tag{41}$$

p_{v2} in Eq. (41) is still given by the saturation pressure at T_2. Equation (41) is an implicit relation because, for $y_1 = y_{1,\text{lim}}$, only two parameters out of p_1, T_1, and g can be specified independently. Equation (41) reduces to Eq. (31) of Ref. 16 in the special case of the pure vapor-droplet mixture ($g=0$).

C. Jump conditions across shock waves with complete evaporation of liquid phase ($y_2=0$)

If the amount of liquid phase in the mixture at the upstream of the shock wave is less than that given by Eq. (41) for a shock wave of a particular strength, then complete evaporation takes place. Upstream of the dispersed wave the medium is an equilibrium mixture of the gas, vapor and liquid, whereas downstream it is a mixture of the gas and superheated vapor. The vapor pressure and the temperature are then independent variables (i.e., they are not connected by the Clausius–Clapeyron equation) and, therefore, neither the approximate jump relations (36)–(38) nor the exact solution (40) derived in Sec. IV A are applicable. Mathematically, the condition $y_2 = 0$ implies $p_{v2} < p_s(T_2)$. The conservation Eqs. (28)–(30) are general and applicable in this case as well. Care must be exercised, however, in determining the mixture enthalpy, density, and pressure.
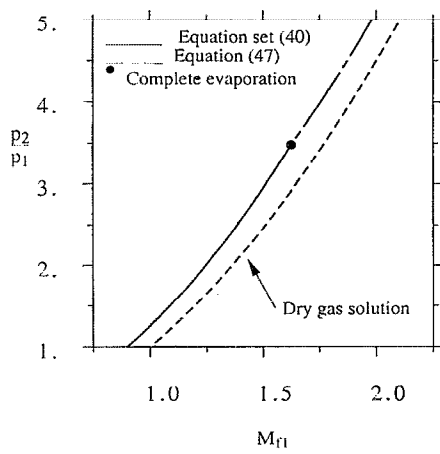
Phys. Fluids, Vol. 6, No. 5, May 1994

Abhijit Guha   1899

FIG. 5. Exact solutions for pressure ratios across aerodynamic shock waves in air–water mixture as a function of upstream frozen Mach number ($p_1 = 1$ bar, $T = 293$ K, $g = 0.95$).

1. An exact solution (for specified p_1, T_1, V_1, and g; $y_2 = 0$)

This is the conventional case when all upstream parameters are known and all the downstream parameters are to be predicted. In this case we can formulate an *exact* analytical solution of Eqs. (28), (29), and (32). We define

$$F_1 = p_1 + \rho_{m1} V_1^2, \tag{42}$$

$$H_1 = \tilde{c}_p T_1 - (1-g) y_1 h_{fg1} + V_1^2/2, \tag{43}$$

$$\tilde{R} = g R_g + (1-g) R_v. \tag{44}$$

Equations (28) and (29) give

$$V_2 = \frac{p_1 + \rho_{m1} V_1^2 - p_2}{\rho_{m1} V_1}. \tag{45}$$

Equations (6) and (32) give

$$H_1 = \frac{\tilde{c}_p}{\tilde{R} \rho_{m1} V_1} p_2 V_2 + \frac{V_2^2}{2}. \tag{46}$$

Substitution of Eq. (45) in Eq. (46) results in a single equation for p_2. The solution is

$$p_2 = \frac{E + \sqrt{E^2 - 4DF}}{2D}, \tag{47}$$

where

$$D = 2\tilde{c}_p/\tilde{R} - 1,$$

$$E = 2F_1(\tilde{c}_p/\tilde{R} - 1),$$

$$F = 2H_1 \rho_{m1}^2 V_1^2 - F_1^2.$$

The pressure increases across an aerodynamic shock wave and, hence, $p_2 > p_1$. This condition eliminates the other root in Eq. (47). Once p_2 is known, V_2 can be calculated from Eq. (45) and T_2 from Eq. (32). Note that Eq. (47) should reduce to the classical Rankine–Hugoniot solution if $y_1 = 0$. (In other words, if the medium just consists of the

inert gas and the superheated vapor, the medium is then a mixture of ideal gases under the assumptions made.)

Equation (47) is plotted for an air–water mixture in Fig. 5. The solution for equilibrium shock waves as discussed in Sec. IV A 2 is also included in the figure and it merges nicely with the curve of Eq. (47) at the point of complete evaporation. The pressure ratio across a frozen shock wave with same values of M_{f1} and g, is also plotted for comparison. It can be seen that the presence of a small quantity of condensable vapor may alter the pressure ratio significantly. (High latent heat of evaporation of water is responsible for this.)

2. An exact solution (for specified p_1, T_1, p_2, and g; $y_2 = 0$)

If, instead of the upstream velocity V_1, p_2 is specified, then also an exact solution of Eqs. (28), (29), and (32) can be obtained. The method of solution is exactly the same as used for deriving Eqs. (27) and (28) in Ref. 16. The solution is

$$T_2 = \frac{2\tilde{c}_p T_1 - 2(1-g) y_1 h_{fg1} + [(p_2 - p_1)/\rho_{m1}]}{2\tilde{c}_p - \tilde{R}[(p_2 - p_1)/p_2]}, \tag{48}$$

$$V_1^2 = \frac{p_2 - p_1}{\rho_{m1}} \left(1 - \rho_{m1} \frac{\tilde{R} T_2}{p_2}\right)^{-1}, \tag{49}$$

where $\tilde{R}$ is given by Eq. (44) and $\tilde{c}_p$ by Eq. (31).

D. Entropy rise through a shock wave

Once conditions upstream and downstream of the dispersed shock wave are established, the increase in mixture specific entropy Δs can be calculated directly from

$$\Delta s = [g s_{g2} + (1-g)(1-y_2) s_{v2} + (1-g) y_2 s_{l2}]$$
$$- [g s_{g1} + (1-g)(1-y_1) s_{v1} + (1-g) y_1 s_{l1}]. \tag{50}$$

In the case of complete evaporation of the liquid phase, y_2 is zero in Eq. (50). Since both the inert gas and the vapor are assumed to behave as perfect gases, Eq. (50) can be expressed in the convenient form

$$\Delta s = \tilde{c}_p \ln\left(\frac{T_2}{T_1}\right) - g R_g \ln\left(\frac{p_{g2}}{p_{g1}}\right) - (1-g) R_v \ln\left(\frac{p_{v2}}{p_{v1}}\right)$$
$$- (1-g) \left(\frac{y_2 h_{fg2}}{T_2} - \frac{y_1 h_{fg1}}{T_1}\right). \tag{51}$$

Figure 6 plots the entropy rise across shock waves corresponding to calculations presented in Fig. 5. The large difference between the curves for wet gas-droplet mixture and dry gas phase suggests that a significant amount of entropy is produced as a result of relaxation mechanism. As an example, the entropy rise in the gas-droplet mixture (with $g = 0.95$) is twice that in the dry gas for an upstream frozen Mach number of 1.75. For details of the mechanism for entropy production inside a dispersed shock wave one may refer to Ref. 16.
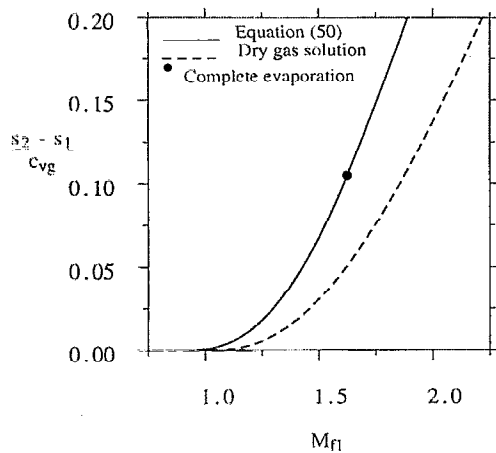
Abhijit Guha

FIG. 6. Entropy rise across aerodynamic shock waves in air–water mixture as a function of upstream frozen Mach number ($p_1 = 1$ bar, $T = 293$ K, $g = 0.95$).

V. CONDENSATION SHOCK WAVES

A. Jump conditions across condensation shocks

If a mixture of an inert gas and a condensable (super-heated) vapor is expanded rapidly (as it flows through a nozzle, blade passage, or over an aerofoil) the vapor does not condense immediately on crossing the saturation line. The vapor becomes sufficiently subcooled until an appreciably high nucleation rate is obtained. Since nucleation rate is a very strong function of the subcooling, the majority of the nuclei are formed within a short region of the Wilson point which is defined as the point of maximum subcooling. When a significant nucleation rate produces sufficient droplet surface area for condensation to occur, the latent heat of condensation starts heating the mixture. As a result, the subcooling decreases very fast (almost exponentially) and the mixture attains (nearly) thermodynamic equilibrium within a short zone (termed the condensation shock). If the variation in the area of the flow passage over this zone of rapid condensation may be neglected, Eqs. (28)–(30) can again be used for giving the jump conditions across condensation shocks (between the Wilson point and the point of attainment of thermodynamic equilibrium). However, care should be taken while evaluating different flow properties.

The mixture of the gas and the condensable vapor upstream of the condensation shock is not in a state of stable thermodynamic equilibrium. The vapor pressure there is not equal to the saturation pressure at the vapor temperature [in fact, $p_{v1} > p_s(T_1)$] and the wetness fraction is not given by the equilibrium value (in fact, $y_1 = 0$). The conservation equations can be solved analytically if all the downstream flow variables are known and the upstream variables are to be predicted. The solution given in Sec. IV C 1 applies in this case with subscripts 1 and 2 being interchanged.

A more convenient boundary condition for an exact analytical solution is specified p_1, T_1, T_2, and g. Since thermodynamic equilibrium is assumed downstream of the

condensation shock, $p_{v2} = p_s(T_2)$. The upstream vapor pressure p_{v1} is related to the mixture pressure through Eq. (10). It is convenient to express the upstream temperature T_1 in terms of the subcooling which is the measure of departure from equilibrium. Thus

$$T_1 = T_s(p_{v1}) - \Delta T_1, \tag{52}$$

where $T_s(p_{v1})$ is the saturation temperature corresponding to the vapor pressure p_{v1} and ΔT_1 is the subcooling at the Wilson point (which constitutes the upstream condition for the condensation shock). The rest of the analysis is the same as in Sec. IV A 2 and the downstream wetness fraction is given by

$$1 - y_2 = \frac{B + \sqrt{B^2 + 4AC}}{2A}, \tag{53}$$

where

$$A = 2(1-g)h_{fg2} - \frac{p_s(T_2) - p_1}{p_s(T_2)} T_2 (1-g) R_v,$$

$$B = 2(1-g)h_{fg2} + 2\widetilde{c}_p [T_s(p_{v1}) - \Delta T_1 - T_2] + g R_g T_2$$

$$+ \frac{p_s(T_2) - p_1}{\rho_{m1}},$$

$$C = \frac{g R_g}{(1-g) R_v} \frac{p_s(T_2)}{\rho_{m1}},$$

$$\rho_{m1} = \frac{p_1}{\widetilde{R}[T_s(p_{v1}) - \Delta T_1]}.$$

The exact value of ΔT_1, at which the Wilson point occurs, depends on the stagnation conditions and the local expansion rate which, in turn, is determined by the shape of the flow passage. (Since nucleation and subsequent growth of droplets are rate processes, higher values of the expansion rate make the mixture deviate further from thermodynamic equilibrium and result in higher ΔT_1 at the Wilson point.) Once y_2 is found, p_2 may be calculated from Eq. (10) and ρ_{m2} from Eq. (6). The flow velocities V_1 and V_2 may then be determined from Eqs. (28) and (29).

Figure 7 plots the pressure ratio p_2/p_1 across condensation shocks in the air–water mixture as a function of upstream frozen Mach number M_{f1}. These curves are calculated quite conveniently by keeping p_1, ΔT_1, and g fixed and by varying T_2 in Eq. (53). Only those solutions which correspond to positive y_2, net entropy rise, and real mass flux, are plotted. [Entropy rise across a condensation discontinuity also can be calculated from Eq. (51).] For the calculations shown in Fig. 7, p_1 is 1 bar and the gas mass fraction is 99% ($g = 0.99$). ΔT_1 for the two sets of curves shown are 30 and 20 K, respectively. In a practical calculation, p_1, T_1, and g will be isentropically related to the upstream stagnation conditions—p_0, T_0, and ϕ_0 (the relative humidity).

Crudely, the effect of condensation may be understood by analogy with external heat addition to an ideal gas flowing through a constant area duct [Eqs. (A1)–(A4), with $dA = 0$]. [*The subtle difference arises because of the deple-*
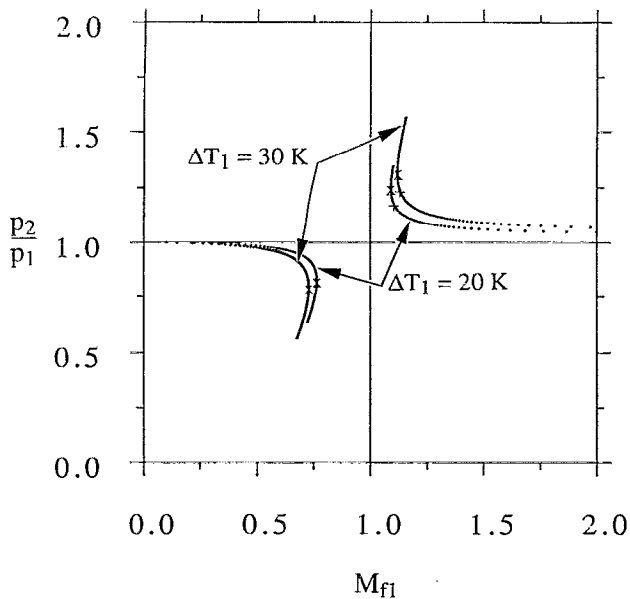
FIG. 7. Pressure ratio across condensation shocks in air–water mixture as a function of upstream frozen Mach number ($p_1 = 2.5$ bar, $g = 0.99$). Symbols: $+$: $M_{f2} = 1$, $\times$: $M_{e2} = 1$.

FIG. 8. Equilibrium Mach number downstream of condensation shocks in air–water mixture as a function of upstream frozen Mach number ($p_1 = 2.5$ bar, $g = 0.99$, $\Delta T_1 = 30$ K). Symbol: $+$: $M_{f2} = 1$.

tion in the mass of the vapor as a result of condensation and the transfer of momentum between the phases. In addition, the amount of heat addition is not an independent variable but depends on the flow conditions. Furthermore, the vapor pressure and the vapor temperature, at thermodynamic equilibrium, are not independent of each other but are connected through the Clausius–Clapeyron equation. Compare Eqs. (65)–(67) with Eqs. (A1)–(A3).] Hence, if ΔT_1 is fixed, the curves for the pressure ratio show two branches for subsonic and supersonic condensation, respectively. When $M_{f1} < 1$, the pressure falls across a condensation shock, whereas, for $M_{f1} > 1$, the pressure rises. This corresponds well with the well-known effects of heat addition. Note that there is a forbidden region near the frozen Mach number of unity (both in the subsonic and supersonic regime). This results from thermal choking because of the liberation of latent heat. Mathematically it manifests in nonreal values for the calculated mass flux. The maximum subsonic and minimum supersonic Mach numbers depend on ΔT_1 and both of them come closer to unity with decreasing ΔT_1. This is because decreasing ΔT_1 results in less amount of heat addition. All this behavior can be seen from Fig. 7.

Figure 7 shows that some values of M_{f1} correspond to two different pressure ratios. To investigate exactly what happens in these cases, we plot (only for the case when $\Delta T_1 = 30$ K) the downstream *equilibrium* Mach number M_{e2} as a function of M_{f1} in Fig. 8. Since thermodynamic equilibrium is assumed downstream of a condensation shock, equilibrium Mach number a_e is the characteristic sonic speed there. It can be seen that the two pressure ratios (corresponding to the same M_{f1}) correspond to subsonic and supersonic downstream conditions. Any point on these curves represents an equilibrium (two-phase) down-
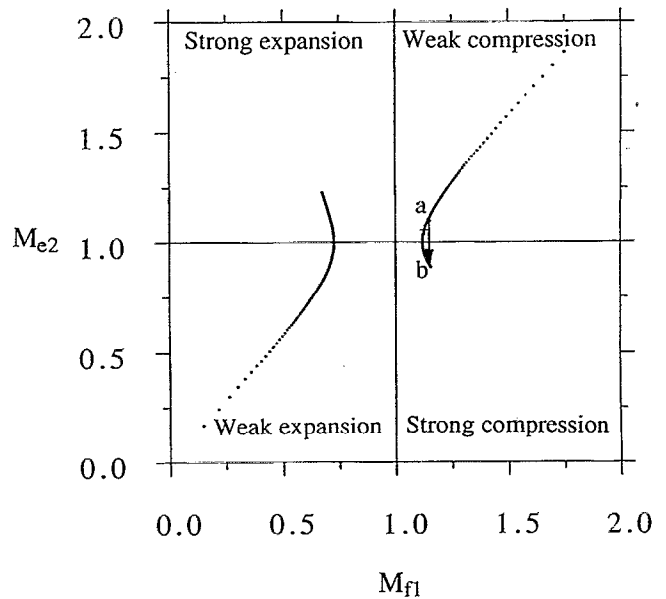
stream condition. Hence, for example, transition from point a to b in Fig. 8 involves a *pure* aerodynamic shock wave and equations developed in Sec. IV A apply between points such as a and b.

To put things in a more familiar perspective, we plot the Hugoniot curve which is the locus of possible downstream pressure p_2 and specific volume v_2 corresponding to fixed upstream pressure and specific volume (Fig. 9). The Hugoniot curve looks similar to the familiar examples of
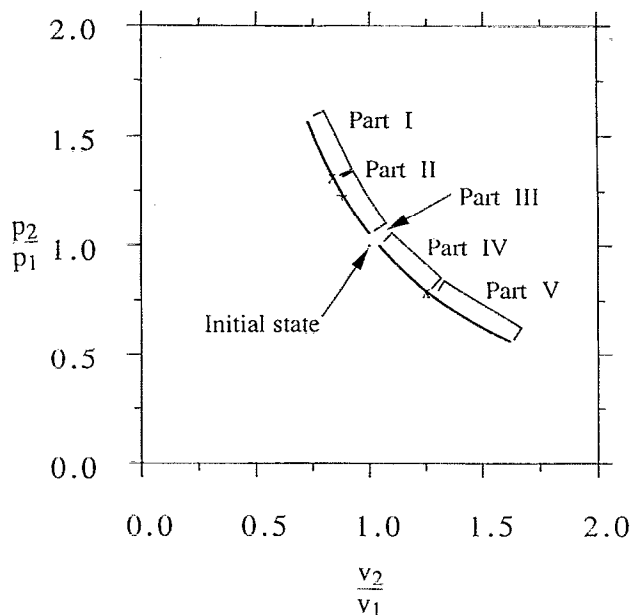

FIG. 9. Calculated downstream states of condensation shocks in air–water mixture with $p_1 = 2.5$ bar, $g = 0.99$, $\Delta T_1 = 30$ K. Symbols: $+$: $M_{f2} = 1$, $\times$: $M_{e2} = 1$.

combustion waves. The points where the downstream flow velocity attains the local equilibrium sonic speed ($M_{e2}=1$) can be called the C–J points, in analogy with the combustion wave theory. Note that the line joining the upstream condition (p_1,v_1) with the lowest point in the upper branch is an isochore, whereas the line joining the upstream condition and the topmost point on the lower branch is an isobar. Also note that the upstream point itself does not lie on the Hugoniot curve as it would do in the case of an adiabatic shock wave in a perfect gas, and that downstream conditions (on the Hugoniot curve) below (p_1,v_1) may correspond to a rise in entropy.

Evidently the Hugoniot curve is divided into five parts [*all of which are calculated by Eq. (53)*]

part I: strong compression $M_{f1} > 1$, $M_{e2} < 1$,

part II: weak compression $M_{f1} > 1$, $M_{e2} > 1$,

part III: forbidden zone Nonreal mass flux,

part IV: weak expansion $M_{f1} < 1$, $M_{e2} < 1$,

part V: strong expansion $M_{f1} < 1$, $M_{e2} > 1$.

In the combustion wave theory, the compression and expansion branches are called detonation and deflagration, respectively. Strong deflagration is a physical impossibility and weak detonation, although not ruled out theoretically, is rare in reality.[26] A strong detonation generally comprises of an adiabatic shock wave followed by a combustion zone.

While the physics of the combustion process is quite similar to that of a condensation shock under present discussion, an important difference should be pointed out clearly. Combustion is an exothermic reaction which becomes more vigorous at higher temperatures. Hence an adiabatic shock wave in front of a combustion zone facilitates combustion by raising the temperature of the mixture of the reactants. Thus, this is normally the flow structure observed in strong detonation waves. On the other hand, *the subcooling of a gas–vapor mixture always decreases in passing through an adiabatic shock wave.* Since nucleation of liquid droplets is a very strong function of the vapor subcooling, an adiabatic shock wave hinders nucleation and might even cause its cessation. Liberation of an appreciable amount of latent heat does not take place unless sufficient number of nuclei are formed and the vapor may need significant further expansion, following an adiabatic shock, to reach the Wilson point (where rapid condensation causes the mixture to return to equilibrium). Thus the flow structure inside a condensation shock wave may be quite different from that of a combustion wave.

The most common type of condensation shock waves reported in the literature, both from experimental (e.g., Ref. 8) and theoretical (e.g., Ref. 5) points of view, falls in the category of part II (weak compression). Weak detonations in a combustible mixture, on the other hand, rarely occur, and slow combustion (weak expansion) is the usual occurrence. Calculations are presented in Sec. V B 2 to show that condensation shock waves in the category of part IV (weak expansion) are also possible. However, for this type of waves to occur through *homogeneous* nucle-

ation in a nozzle, the vapor may have to be subcooled at the inlet stagnation condition. A recent article[27] describes subsonic condensation (heterogeneous condensation on cloud condensation nuclei, CCN) of moist air in very long intake ducts of jet engines during stationary operation. The theory presented in this section can be applied directly across such condensation zones.

One can discount the possibility of a strong expansion (part V) because heat transfer alone cannot accelerate a flow from subsonic to supersonic velocities and, therefore, a strong expansion must include an expansion shock wave. Such a shock wave structure is internally unstable and is not evolutionary. (This is true both for combustible mixtures as well as for condensation shocks. However, note that the parts of part V shown in Figs. 7–9 do not contravene the second law of thermodynamics. A strong expansion in an ideal gas, on the other hand, would have resulted in a decrease in entropy.) Landau and Lifshitz[26] suggest that the remaining category of condensation shocks (strong compression, part I) is not normally achievable because the system is overdetermined in this case. However, they reckon that a condensation discontinuity with $M_{f1} > 1$, $M_{e2} < 1$ may actually (for certain conditions of vapor content and shape of the surface past which the flow occurs) be simulated by a true condensation discontinuity with $M_{f1} > 1$, $M_{e2} > 1$, closely followed by a shock wave which renders the flow subsonic. A flow structure such as this is plausible if the condensation shock is close to the usual trailing-edge shock waves in a transonic turbine blade row.[28] In the next section we will show that, depending on the flow conditions, the condensation zone may involve an *embedded* frozen shock wave as well, as opposed to a separate shock wave downstream of the condensation zone as envisaged by Landau and Lifshitz.

Figures 10 and 11 plot the entropy rise across condensation shocks and the mass fraction of the condensed phase, respectively. As with the aerodynamic shock waves, the entropy rise across condensation shock waves is also given by Eq. (51). The symbol × in Figs. 7–11 correspond to a downstream *equilibrium* Mach number of unity ($M_{e2}=1$). Similarly, the symbol + in Figs. 7–11 correspond to a downstream *frozen* Mach number of unity ($M_{f2}=1$). The equilibrium, control-volume analysis of this section suggests that the line segment between × and + represent viable condensational jumps. It has, however, been shown in Appendix B (also see Refs. 18 and 19) that the nonequilibrium variables such as subcooling and velocity slip show unstable behavior when the flow velocity lies in this range. Thus consideration of nonequilibrium gas dynamics abandon these solutions which are permitted by an integral analysis.

The condensation discontinuity is obviously not arbitrarily triggered at any location in the flow field. It occurs only when the subcooling attained is sufficient (in respect of the expansion rate) to cause significant nucleation of liquid droplets and where the local flow velocity sustains it as a stable structure. It may also be recalled that the above discontinuous model of condensation assumes no variation in flow area within the zone of condensation, and, there-
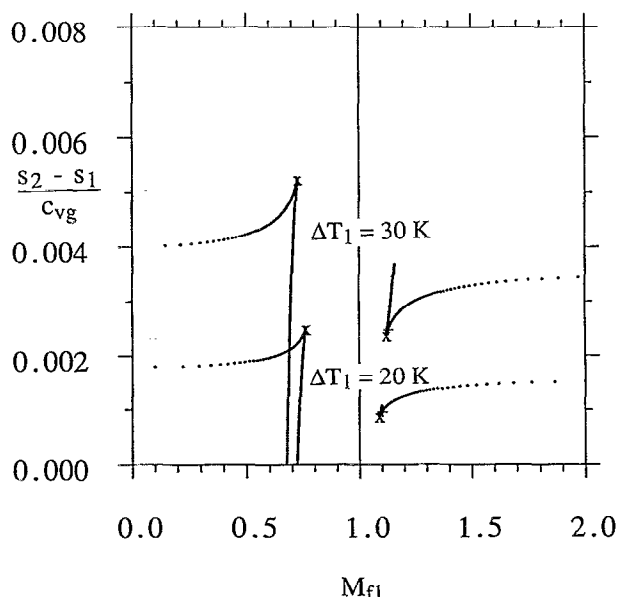
Phys. Fluids, Vol. 6, No. 5, May 1994

Abhijit Guha   1903

FIG. 10. Entropy rise across condensation shocks in air–water mixture as a function of upstream frozen Mach number ($p_1 = 2.5$ bar, $g = 0.99$). Symbols: +: $M_{f2} = 1$, ×: $M_{e2} = 1$.

fore, sometimes may not be directly applicable to condensing nozzle flows. (References 29 and 30 discuss asymptotic theories describing conditions under which the final collapse of the supersaturated state can be described by a condensation shock.) Despite this limitation, the model provides valuable physical insight and can sometimes be applied directly for quantitative predictions. (For example, an application area, cited above, is the condensation of moist air in long intake ducts of jet engines during stationary operation. Reference 31 discusses applications in nozzle flows.) In the next section, we present example calculations for different types of condensation shock waves in pure steam flowing through a convergent–divergent nozzle.

In order to conclude this section, we note that all these complexities and different regimes of condensation shock waves did not arise in the case of aerodynamic shock waves in gas–vapor-droplet flow as discussed in Sec. IV. The only boundary condition compatible with stability and the second law of thermodynamics consists of a supersonic flow at the upstream of the aerodynamic shock wave and a subsonic flow at the downstream ($M_{e1} > 1$, $M_{e2} < 1$ if complete evaporation does not take place).

B. Condensation shock waves in convergent–divergent nozzles

The integral analysis of the previous section only relates the upstream and downstream conditions across condensation shock waves. If, on the other hand, one is interested in the details of the variation of different flow variables *within* a condensation shock wave, differential equations of motion must be solved. In Sec. V B 1 we present one-dimensional gasdynamic equations incorporating *all* the relaxation processes arising out of nonequilib-

rium transfer of mass, momentum, and energy between the vapor and the liquid phase. In Sec. V B 2 we present solution methods and example calculations.

1. Nonequilibrium gasdynamic equations for steady, pure vapor-droplet flow and conditions for thermal choking

For simplicity, we consider pure substances only. This means that the vapor consists of the same chemical species as the liquid droplets and that no carrier gas is present. We adopt the usual "two-fluid" model and view the liquid droplets as providing sources or sinks of mass, momentum, and energy for the vapor, each source term varying continuously in the x direction. The combined liquid and vapor continuity, momentum, and energy equations are, respectively, given by

$$\frac{d}{dx}\left[A\left(\rho_v V_v + \frac{y}{1-y}\rho_v V_l\right)\right] = 0, \tag{54}$$

$$A\frac{dp}{dx} + \frac{d}{dx}\left[A\left(\rho_v V_v^2 + \frac{y}{1-y}\rho_v V_l^2\right)\right] = 0, \tag{55}$$

$$\frac{d}{dx}\left[A\rho_v V_v\left(h_v + \frac{1}{2}V_v^2\right) + \frac{y}{1-y}A\rho_v V_l\left(h_l + \frac{1}{2}V_l^2\right)\right] = 0, \tag{56}$$

where h is the enthalpy, ρ_v is the vapor phase density, V is the velocity, y is the wetness fraction, A is the flow cross-sectional area, and x is the distance measured in the flow direction. The subscripts v and l refer to the vapor and liquid phase, respectively. The equation set (54)–(56) is incomplete and must be complemented by three equations representing the interphase mass, momentum, and energy transfer. The interphase transfer mechanisms are quanti-
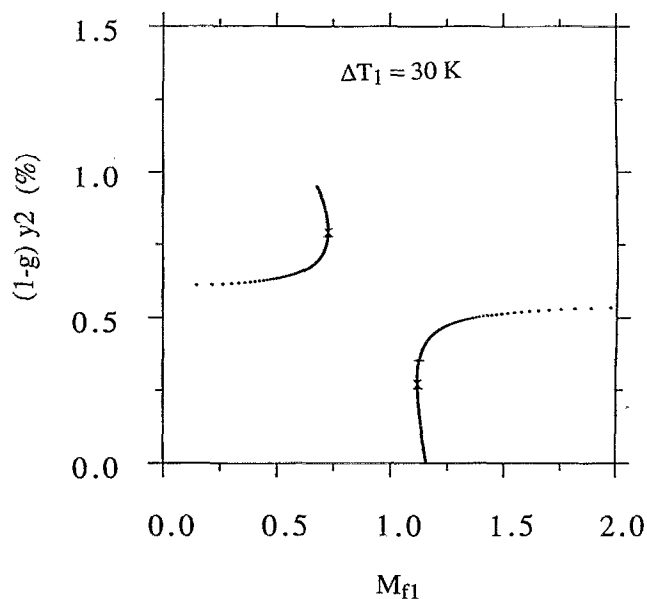

FIG. 11. Mass fraction of liquid phase condensed across condensation shocks in air–water mixture as a function of upstream frozen Mach number ($p_1 = 2.5$ bar, $g = 0.99$). Symbols: +: $M_{f2} = 1$, ×: $M_{e2} = 1$.

Abhijit Guha

fied in terms of relaxation times which represent the rates at which the two-phase system reverts to equilibrium following a disturbance. As nonequilibrium variables, we choose $\Delta V = V_v - V_l$ to represent velocity (or inertial) relaxation, $\Delta T_l = T_s - T_l$ to represent droplet temperature relaxation, and $\Delta T = T_s - T_v$ to represent vapor thermal relaxation. (Here, T_s is the saturation temperature at pressure p, and ΔT represents the negative of the vapor superheat.) It is shown in detail by Young and Guha[19] that the interphase transfer equations can then be written as

$$\frac{dT_l}{dx} = \frac{T_{l\infty} - T_l}{V_l \tau_D}, \tag{57}$$

$$\frac{dV_l}{dx} = \frac{V_v - V_l}{V_l \tau_I}, \tag{58}$$

$$(h_v - h_l) n \frac{dm}{dx} = \frac{(1-y)c_{pv}(T_{l\infty} - T_v)}{V_l \tau_T} + \frac{yc_l(T_{l\infty} - T_l)}{V_l \tau_D}, \tag{59}$$

where m is the mass of a liquid droplet and n is the number of droplets per unit mass of the mixture, and are related to the wetness fraction via $y = nm$. τ_D, τ_I, and τ_T are different relaxation times and their expressions are given by

$$\tau_I = \frac{2r^2 \rho_l}{9\mu_v} [\phi(\text{Re}) + 4.5 \text{ Kn}], \tag{60}$$

$$\tau_D = \left(\frac{2-q_c}{2q_c}\right)\left(\frac{R_v T_s}{h_{fg}}\right)^2 \left(\frac{\gamma \rho_l c_l}{3R_v}\right)\frac{\sqrt{2\pi R_v T_s}}{p}, \tag{61}$$

$$\tau_T = \frac{(1-y)c\rho_v \rho_l r^2}{3\lambda_v y}(1 + 4.5 \text{ Kn/Pr}), \tag{62}$$

where $\phi(\text{Re})$ is an empirical correction for large slip Reynolds numbers ($\text{Re} = 2\rho_v r |\Delta V| / \mu_v$) given by

$$\phi(\text{Re}) = [1 + 0.15 \text{ Re}^{0.687}]^{-1} \tag{63}$$

and λ_v and μ_v are the vapor thermal conductivity and dynamic viscosity, respectively, q_c is the condensation coefficient, Pr is the vapor Prandtl number and $\text{Kn} = l_v/2r$ is the droplet Knudsen number, l_v being the molecular mean free path of the vapor, and r the radius of the droplet. In most situations, the steady-state droplet temperature $T_{l\infty}$ is close to the saturation temperature T_s if the capillary subcooling ($\Delta T_{\text{cap}} = 2\sigma_s T_s / r\rho_l h_{fg}$, where σ_s is the surface tension) is negligible. (The Kelvin–Helmholtz equation shows that in steam–water mixture the capillary subcooling is 0.43 °C if the droplet radius is 0.05 μm and 0.01 °C if the radius is 2 μm.) Young and Guha[19] have discussed, at length, the assumptions involved in the derivation of the relaxation times and have indicated their range of validity. Equations (60)–(62) are supposedly valid for all droplet Knudsen numbers from the continuum to the free molecule regime. For example, for small slip Reynolds numbers and continuum flow (Re≪1, Kn≪1) Eq. (60) reduces to the Stokes drag formula for a sphere. For free molecule flow (Kn≫1) an expression derivable from kinetic theory is obtained. The expression within the bracket in Eq. (60) provides a simple interpolation formula for intermediate

Knudsen numbers. Similarly, for small Kn, Eq. (62) reduces to the continuum expression for steady-state heat transfer from a sphere. For large Kn the kinetic theory (free molecule) result is regained. The method of analysis presented in this article is not dependent on the forms of Eqs. (60)–(62), however, and other, possibly more suitable, expressions could easily be incorporated if desired.

As a result of our assumption that each individual droplet retains its identity (Sec. I), the number of droplets is conserved (in non-nucleating flow). The conservation is expressed by

$$\frac{d}{dx}\left(\frac{n\rho_v A V_l}{1-y}\right) = 0. \tag{64}$$

Inside the nucleation zone, obviously Eq. (64) is not valid and one needs an equation specifying the rate of formation of new droplets. Note that, while writing Eqs. (54)–(64), we have tacitly assumed that the droplets are monodispersed. A polydispersed droplet population is normally represented by discretizing the distribution into a number of droplet groups. One would then require one equation set (57)–(64) for each droplet group, and the contribution from all the droplet groups have to be summed over while writing the conservation equations (54)–(56).

Equations (54)–(64) may be combined (after neglecting second order small terms involving the products of any two of $\Delta V/V_v$, $\Delta T/T_v$, and $\Delta T_l/T_s$) to give explicitly the variation in different vapor properties:

$$(1-M_f^2)\frac{DV_v}{V_v} = -\frac{DA}{A} + \left(1 - \frac{c_{pv}T_s}{h_{fg}}\right)\Theta + M_f^2 \Pi - \sigma, \tag{65}$$

$$(1-M_f^2)\frac{Dp}{p} = \gamma M_f^2 \left[\frac{DA}{A} - \left(1 - \frac{c_{pv}T_s}{h_{fg}}\right)\Theta - \Pi + \sigma\right], \tag{66}$$

$$(1-M_f^2)\frac{DT_v}{T_v} = (\gamma - 1)M_f^2 \frac{DA}{A} + \left[1 - \gamma M_f^2\left(1 - \frac{R_v T_s}{h_{fg}}\right)\right]\Theta$$
$$- (\gamma - 1)M_f^2 \Pi + (\gamma - 1)M_f^2 \sigma, \tag{67}$$

where the shorthand notation $D = d/dx$ is used for convenience. The variables Θ, Π, and σ represent the contributions from three relaxation phenomena and are given by

$$\Theta = \frac{\Delta T}{V_v \tau_T T_v}, \tag{68}$$

$$\Pi = \frac{y}{1-y}\frac{\Delta V}{V_v \tau_I V_v}, \tag{69}$$

$$\sigma = \frac{y}{1-y}\frac{c_l T_s}{h_{fg}}\frac{\Delta T_l}{V_v \tau_D T_s}. \tag{70}$$

Here, Θ is associated with vapor thermal relaxation, Π with inertial (or velocity slip) relaxation, and σ with droplet temperature relaxation. [If the capillary subcooling, ΔT_{cap}, is not negligible, then ΔT and ΔT_l in Eqs. (68) and (70) should be replaced by ($\Delta T - \Delta T_{\text{cap}}$) and ($\Delta T_l - \Delta T_{\text{cap}}$), respectively.] It is easy to draw from Eqs. (65)–(67) a table of influence coefficients for nonequilibrium condensing flow (Table I). Comparison of Eqs. (65)–(67) with Eqs. (A1)–(A3) shows the similarities

TABLE I. Sign of influence coefficients in condensing flow. In a continually expanding flow, in general, $\Theta>0$, $\Pi>0$, and $\sigma<0$.

	$M_f<1$ Contribution from				$M_f>1$ Contribution from			
	DA/A	Θ	Π	σ	DA/A	Θ	Π	σ
DV_v/V_v	$\mp$ᵃ	+	+	+	$\pm$ᵃ	−	−	−
Dp/p	$\pm$ᵃ	−	−	−	$\mp$ᵃ	+	+	+
DT_v/T_v	$\pm$ᵃ	+ if $M_f<M_*$ᵇ − if $M_f>M_*$	−	−	$\mp$ᵃ	+	+	+

ᵃUpper sign if $DA>0$, lower sign if $DA<0$.
ᵇIn an ideal gas $M_*=1/\sqrt{\gamma}$. Equation (67) shows that in a condensing flow, $M_*=\{\gamma[1-(R_vT_s/h_{fg})]\}^{-1/2}$.

and differences between the characteristics of a condensing flow and the flow of an ideal gas with external heat addition. In particular, note that the mass depletion due to condensation and the use of the Clausius–Clapeyron equation (to obtain the vapor temperature) result in terms like $[1-(c_{pv}T_s/h_{fg})]$ and $[1-(R_vT_s/h_{fg})]$ in the flow equations. (These could give unusual results in fluids with $c_{pv}T_s/h_{fg}>1$, or, $R_vT_s/h_{fg}>1$.)

The general expressions for the variation of the subcooling, ΔT, and the frozen Mach number, M_f, can be derived from Eqs. (65)–(67):

$$(1-M_f^2)\frac{1}{T_v}\frac{d(\Delta T)}{dx}+\left(1-\frac{M_f^2}{M_+^2}\right)\Theta$$
$$=M_f^2(\gamma_v-1)\left(1-\frac{c_{pv}T_s}{h_{fg}}\right)\left(-\frac{1}{A}\frac{dA}{dx}+\Pi-\sigma\right), \tag{71}$$

$$(1-M_f^2)\frac{1}{M_f}\frac{dM_f}{dx}$$
$$=\left(1+\frac{\gamma_v-1}{2}M_f^2\right)\left(-\frac{1}{A}\frac{dA}{dx}-\sigma\right)+\frac{\gamma_v+1}{2}M_f^2\Pi$$
$$+\left\{\frac{1}{2}\left[1+\gamma M_f^2\left(1-\frac{R_vT_s}{h_{fg}}\right)\right]-\frac{c_{pv}T_s}{h_{fg}}\right\}\Theta, \tag{72}$$

where M_f is the frozen Mach number. M_+ in Eq. (71) is given by

$$M_+=a_+/a_f, \tag{73}$$

$$\left(\frac{a_+}{a_f}\right)^2=\left[\gamma_v\left(1-2\frac{R_vT_s}{h_{fg}}+\frac{R_vT_s}{h_{fg}}\frac{c_{pv}T_s}{h_{fg}}\right)\right]^{-1}. \tag{74}$$

Equation (74) shows that the ratio a_+/a_f is a weak function of pressure and *does not depend on the wetness fraction*. For wet steam, $a_+/a_f\approx0.92$ over a rather wide range of conditions (the ratio varies from 0.919 at 0.1 bar to 0.934 at 2 bars). Note that

$$a_+\approx a_e/\sqrt{1-y}=\sqrt{\gamma_e/\gamma_v}a_f, \tag{75}$$

where the equilibrium speed of sound, a_e, and the equilibrium isentropic index, γ_e, are given by Eqs. (27) and (25), respectively.

Equations (71) and (72) show that, depending on the shape of the flow passage and the flow conditions, quite complicated variations in ΔT and M_f are possible. (We, however, discuss, in the next section, only those cases which are found to occur in numerical calculations in nozzles of ordinary shapes. More exotic cases are left as a mathematical fun.) Equation (72) also shows that, when *all the nonequilibrium processes are properly taken care of, the condition of thermal choking is obtained when the frozen Mach number is unity.* Simplifications of the flow equations may lead to misinterpretations. For example, if droplet temperature equilibration (with frozen interphase momentum and heat transfer) is assumed and then the differential equations are rederived systematically, the common factor $(1-M_f^2)$ appearing in the left hand side of Eqs. (65)–(67), and (71)–(72) is replaced by another common factor $(1-V_v^2/a'^2)$, where the characteristic speed of sound a' is given by Eq. (B2). Similarly, the assumption of equilibrium droplet temperature and velocity slip (with frozen heat transfer) results in a common factor $(1-V_v^2/a''^2)$, where the characteristic speed of sound a'' is given by Eq. (B5). Finally, the assumption of full equilibrium results in a common factor $(1-V_v^2/a_e^2)$, where a_e is the equilibrium speed of sound. Clearly, *although these simplified models give mathematical singularities when the flow velocity equals a', a'', and a_e, respectively, they do not correspond to the physical condition of choking.* [Note that many equations found in the literature are prone to misinterpretations. For example, compare Eqs. (4)–(7) given by Barschdorff and Fillipov[6] with Eqs. (65)–(67) derived here.]

2. Calculation of different types of condensation shock waves in nozzles and discussion

Equations presented in Sec. V B 1 are general and should be used for accurate solutions. Mathematical equations in this full form must be considered for drawing correct physical conclusions such as determining the condition of thermal choking. However, the size of the droplets formed through homogeneous nucleation is very small (usually less than 1 μm). Equations (60) and (61) show that the relaxation times τ_I and τ_D for tiny droplets are very small,[18] and any practical computational scheme based on these full equations consumes unacceptably large amount of CPU time. A compromise is usually made by assuming complete equilibration of velocity slip and droplet temperature relaxation. The slip velocity for small droplets is generally negligible and *finite volume* formulation of the resulting equations can capture many overall flow features. (However, the full equations should be kept in mind and the effects of any approximation appreciated. Sometimes the approximations, e.g., of velocity slip equilibration, may lead to great inaccuracies. This would be the case if, for example, the droplets are large and the vapor is substantially wet at the nozzle inlet.)

A direct result of the assumption of equal phase velocity is that the continuity, momentum, and energy equations become similar to their single-phase counterparts, if the mixture density ρ_m and the mixture specific enthalpy $\bar{h}$ are

Abhijit Guha

used. The mixture density is connected to the vapor density [neglecting the volume of the liquid phase as before, with $g=0$ in Eq. (1)]

$$\rho_m = \rho_v / (1-y) \tag{76}$$

and the mixture specific enthalpy is

$$\bar{h} = (1-y)h_v + yh_l, \tag{77}$$

where h_v and h_l are the specific enthalpies of the vapor and the liquid phase, respectively. With these definitions and *the assumption of no velocity slip*, the gasdynamic equations for inviscid adiabatic unsteady two-phase flow becomes

$$\text{continuity} \quad \frac{\partial \rho_m}{\partial t} + \nabla \cdot (\rho_m \mathbf{V}) = 0, \tag{78}$$

$$\text{momentum} \quad \frac{\partial \mathbf{V}}{\partial t} + (\mathbf{V} \cdot \nabla)\mathbf{V} + \frac{\nabla p}{\rho_m} = 0, \tag{79}$$

$$\text{energy} \quad \frac{\partial}{\partial t}\left[\rho_m\left(\bar{e} + \frac{V^2}{2}\right)\right] + \nabla \cdot \left[\rho_m \mathbf{V}\left(\bar{h} + \frac{V^2}{2}\right)\right] = 0, \tag{80}$$

where the vector quantity $\mathbf{V}$ is the common velocity of the two phases and $\bar{e}$ is the specific internal energy of the mixture. Equations (78)–(80) are identical to those describing the adiabatic flow of an inviscid single-phase fluid and are valid for unsteady, three-dimensional flow. *The differences are apparent, however, when it is recalled that the wetness fraction y in Eqs. (76) and (77) is not necessarily the equilibrium value and that h_v and h_l in Eq. (80) are evaluated at temperatures T_v and T_l which are not necessarily equal to the local saturation value T_s.* Departure from thermodynamic equilibrium must be allowed in calculations for non-equilibrium condensation. One needs a nucleation rate equation specifying the production rate of new droplets and a droplet growth law [e.g., Eq. (59)] specifying the rate of condensation (or evaporation) on existing droplets [providing the nonequilibrium value of y to be used in Eqs. (76) and (77)]. Both the rates of nucleation and droplet growth depend on the local subcooling.

[In passing, it should be noted that if the conservation equations were expressed in terms of vapor density ρ_v and vapor enthalpy h_v, then mass depletion due to condensation, interphase drag force, and condensational heat release should appear as source (or sink) terms, respectively, in the continuity, momentum, and energy equations for the vapor phase. Sometimes the equations found in the literature mix the above two approaches and, therefore, constitute an inconsistent formulation (e.g., Ref. 10).]

One of the most effective methods of calculation is to write a computational "black box" which contains the nucleation and droplet growth equations, and the energy equation in its thermodynamic form. [*The equation $d\bar{h} - dp/\rho_m = 0$, derivable from Eqs. (78)–(80), does not necessarily imply zero entropy increase in multiphase flow.*] Together they furnish the full set of equations that describe completely the formation and growth of liquid droplets in a fluid particle (from a Lagrangian viewpoint) if the pressure–time variation is specified. The pressure–time variation is obtained by the time marching solutions of the conservation equations such as Denton's method,[32] extensively used for single-phase calculations in turbomachinery blade rows. In this respect, the thermodynamic aspects of phase change can be completely divorced from fluid dynamical considerations so that the use of the "black box" is effectively independent of any particular computational fluid dynamics (CFD) application. Thus established single-phase CFD codes can, rather easily, be modified to deal with nonequilibrium two-phase flow with the above-mentioned *modular approach*. (The flexibility of this scheme may be appreciated from Ref. 33 where the same "black box" has been grafted into a streamline curvature calculation procedure.)

The development of the computational routines within the "black box" represents a comparatively major undertaking and has been fully described by Guha and Young.[5] The routines are sufficiently general and robust to deal with any type of nucleating or wet steam flow and (in contrast to many procedures reported in the literature) *full details of the droplet size spectrum following nucleation are retained in the calculations*. The last aspect is essential for accurate modeling of the nucleation zone. Successive nucleations after the primary are dealt with as a matter of course should the expansion be sufficiently rapid to generate the high levels of subcooling required. The computational scheme has been validated against measurements of steady (both sub- and supercritical) and unsteady condensation shock waves.[5] Here, we present calculations for different types of steady condensation shock waves in *pure steam*.

Figure 12 shows condensation in a one-dimensional convergent–divergent nozzle for five different inlet conditions. For all cases, the inlet total pressure p_0 is kept constant while the inlet total temperature T_0 is varied. The back pressure is kept sufficiently low so that the flow is supersonic over (at least) some part of the diverging section. The figure gives the variation of static pressure, degree of subcooling, and frozen Mach number along the nozzle axis. As discussed in Sec. V A (see also Appendix A), the variation of the flow properties of the vapor phase can be explained *approximately* by considering the (often competing) effects of change of area and external heat transfer. The position and structure of the condensation shock depends on the shape of nozzle and the stagnation conditions, which together determine the flow conditions and the heat release rate due to condensation.

Consider Fig. 12. If the stagnation temperature T_0 is very high, then no appreciable nucleation takes place over the length of the nozzle and dry steam expands similar to the isentropic expansion of a perfect gas (even though steam might have become subcooled at the exit of the nozzle). The corresponding variation of pressure and frozen Mach number have been marked as "isentropic" in Fig. 12, and constitute the datum line for understanding the effects of nonequilibrium condensation.
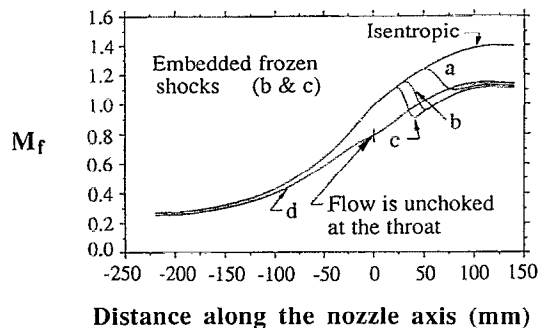
If the initial superheat at nozzle inlet is decreased (by lowering T_0), the "condensation shock" occurs somewhere in the diverging section of the nozzle (curve a in Fig. 12).
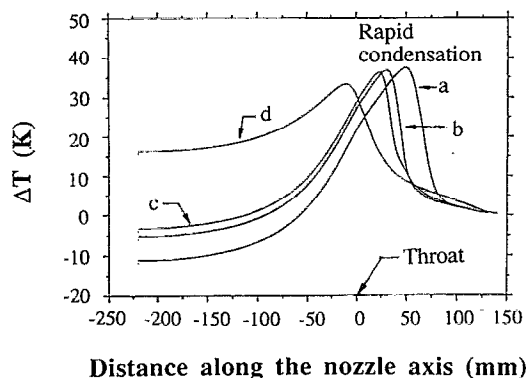
Phys. Fluids, Vol. 6, No. 5, May 1994

Abhijit Guha   1907
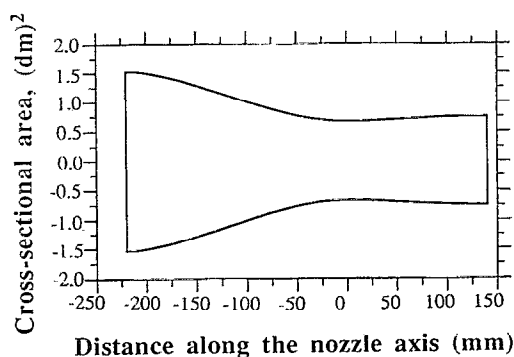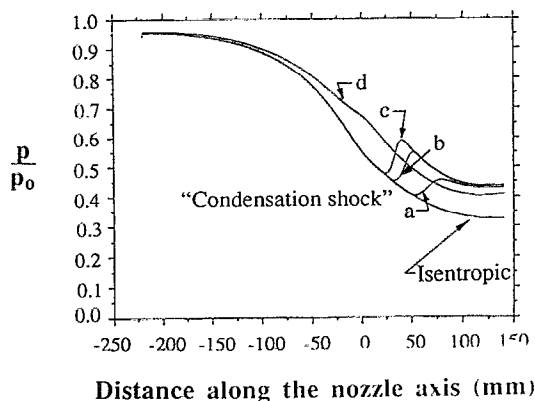
FIG. 12. Time-marching solution of different condensational flow regimes in steady nozzle flow of pure steam ($p_0=0.3514$ bar for all curves): (a) $T_0=362$ K, (b) $T_0=354$ K, (c) $T_0=352$ K, (d) $T_0=332$ K) (i) Dimensions of the nozzle, (ii) variation of pressure ratio, (iii) variation of frozen Mach number, and (iv) variation of subcooling.

The flow has become supersonic at the onset of condensation. Inside the condensation zone the effect of heat addition exceeds that of area change, and so the flow velocity decreases. The velocity remains, however, above the local frozen speed of sound. Downstream of the zone of condensation the area change becomes dominant and so the Mach number increases again (the flow being supersonic). This is the regime of the so-called subcritical heat addition ($M_{f1}>1,M_{f2}\gg1$) which involves continuous variation in flow properties.

It can be seen (curve a, Fig. 12) that, at first, ΔT increases continuously due to expansion. The steam is superheated at the nozzle inlet, passes through the saturation temperature ($\Delta T=0$), and becomes highly subcooled until the total surface area of the freshly nucleated droplets is sufficient to give rise to a significant rate of heat transfer. At this point, the liberated latent heat starts heating the vapor and the subcooling drops very fast (rapid condensation zone). The heat transfer rate is proportional to the prevailing subcooling. Therefore, as the subcooling decreases, the heat transfer rate also simultaneously decreases and, at some point, the effects of area change assume dominance. The point of maximum subcooling is termed the Wilson point. It represents the practical end of

the nucleation process, as according to classical nucleation and droplet growth theory no embryo can grow against a negative gradient of subcooling. Figure 12 also shows that the frozen Mach number at the Wilson point is only slightly different from the Mach number at the same location in the isentropic case.

If T_0 is reduced further (keeping p_0 constant), the steam would attain saturation earlier in the nozzle and consequently the condensation shock wave would appear closer to the throat. The frozen Mach number at the Wilson point decreases and the change in flow properties, e.g., pressure, becomes steeper [primarily because of the $(1-M_f^2)$ terms in the denominator of Eqs. (A1)–(A4)]. The frozen Mach number at the end of the condensation zone comes closer to unity. By extrapolation of this reasoning it can be argued that, for a particular inlet superheat, the Mach number at the end of the condensation zone will be exactly equal to unity ($M_{f2}=1$). The flow is then said to be thermally choked. There are two sonic points in this case: one at the geometric throat of the nozzle and the second at the point of thermal choking. If the inlet superheat is reduced any further than this critical value, no continuous variation of flow parameters is possible.

However, a steady solution may arise under these con-
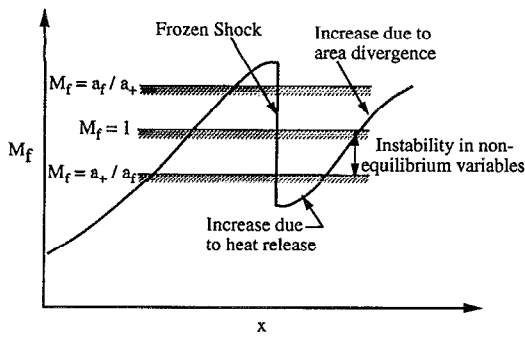
Abhijit Guha

FIG. 13. Schematic structure of a supercritical condensation shock wave.

ditions by the formation of a Rankine–Hugoniot aerodynamic shock wave *inside* the condensation zone. Condensation with this type of inbuilt frozen shock is generally called supercritical condensation shock. Curves b and c in Fig. 12 illustrate two examples of supercritical condensation. The frozen shock takes the velocity below the frozen speed of sound; the flow then accelerates due to the remaining heat release, and, once M_f is unity, accelerates further due to the diverging flow area. Equations (71) and (72) specify the continuous variation of subcooling and frozen Mach number in the nozzle. It may be seen that the effects of area change and heat transfer are very delicately balanced when the Mach number is close to unity. The flow adjusts the location of the frozen shock so as to give rise to a stable structure.

Figure 13 schematically shows a limiting case of supercritical condensation where the frozen shock occurs immediately after the Wilson point. A study of Eq. (71) reveals that the subcooling shows unstable behavior ($|\Delta T|$ grows irrespective of the magnitude of the relaxation time) when the flow velocity lies between a_f and a_+. Because of this inherent instability, the downstream condition of the frozen shock cannot lie within a_f and a_+ with a substantial residual ΔT. The frozen Mach numbers upstream (subscript 1) and downstream (subscript 1') of the frozen shock wave are related by the classical Rankine–Hugoniot relations

$$M_{f1'}^2 = \frac{1 + [(\gamma_f - 1)/2]M_{f1}^2}{\gamma_f M_{f1}^2 - [(\gamma_f - 1)/2]} . \tag{81}$$

The decrease in subcooling across a frozen shock (with upstream Mach number M_{f1}) can be calculated from standard Rankine–Hugoniot relations and the Clausius–Clapeyron equation. Hence

$$\Delta T_{1'} = \Delta T_1 - T_1 \frac{2\gamma_f}{\gamma_f + 1} (M_{f1}^2 - 1)$$

$$\times \left[\frac{\gamma_f - 1}{\gamma_f + 1} \left(1 + \frac{1}{\gamma_f M_{f1}^2} \right) - \frac{R_v T_s}{h_{fg}} \right]. \tag{82}$$

It is normally argued[3,4,6,31,34] that the frozen shock wave occurs when $q > q_{\text{crit}}$, where the critical amount of heat q_{crit} is given by Eq. (A5). However, this argument is somewhat fallacious. First of all, this argument is derived

by analogy with external heat transfer to a single-phase ideal gas and Eq. (A5) is valid only for such flows in constant area ducts. A vapor-droplet medium is complicated because there is no unique sonic speed[18] and the amount of heat addition is not an independently controllable variable. Further complexities arise because of interphase mass and momentum transfer. [Compare Eqs. (65)–(72) with (A1)–(A4).] Hence the results from gasdynamics of a single-phase ideal gas [Eq. (A5)] cannot be applied directly to vapor-droplet flow. Second, the assumption of constant area while deriving Eq. (A5) may not correspond well to the case of supercritical condensation where there is a very delicate balance between the effects of area change and the heat release. (An expression for q_{crit} in condensing flow, taking into account the mass depletion and the area variation, is given in Ref. 35.) Finally, the conclusion that $q > q_{\text{crit}}$ would give rise to an adiabatic shock wave is not true even for the flow of an ideal gas. The analysis of Appendix A shows clearly that the presence of an inbuilt shock wave does not increase the heat absorption capacity. [According to Eq. (A5), q_{crit} at M_{f1} ($M_{f1} > 1$) is exactly the same as q_{crit} at M_{f2} ($M_{f2} < 1$) if M_{f1} and M_{f2} are related by the classical Rankine–Hugoniot equations.]

The mass fraction of the liquid phase downstream of the condensation shock, y_2, depends on the integral $\int \Delta T dx/V$ [Eq. (59)]. Since ΔT decreases discontinuously across a frozen shock [Eq. (82)], the magnitude of the above integral decreases when a frozen shock wave is present, thereby decreasing the amount of liquid condensed. The amount of heat addition in a condensation shock wave is approximately given by $h_{fg} y_2$. The presence of a frozen shock inside the condensation zone, therefore, actually *decreases* the release of latent heat. The resulting decrease in the rise in entropy counteracts the additional source of entropy generation due to the frozen shock. This is why the total rise in entropy across a supercritical condensation shock is comparable to that across a subcritical one (as reported by Skillings[34]).

Under certain conditions the frozen shock described above may become unstable and propagate towards the nozzle throat. The compressive wave ultimately interferes with the nucleation zone causing a reduction in nucleation rate and hence heat release rate. With the cause of its inception removed, the strength of the wave decreases and the flow again expands through the throat in a shock-free manner thus allowing the whole process to repeat itself. Such unsteady flow is normally observed in pure steam when the inlet stagnation temperature T_0 is close to the saturation temperature at the the inlet stagnation pressure p_0. Numerical calculations of oscillating flows and comparison with experiments may be found in Ref. 5. Here we do not consider this unsteady flow behavior any further.

If T_0 is reduced sufficiently (below the saturation temperature), a steady flow is obtained but the flow structure changes completely (curve d in Fig. 12). The flow is unchoked at the nozzle throat, as is evident from the Mach number distribution. Changes in the flow variables have thus been affected all the way up to the inlet thereby alter-

Phys. Fluids, Vol. 6, No. 5, May 1994

Abhijit Guha   1909

TABLE II. Variation of M_f and ΔT in condensing nozzle flow.

Converging section	
$M_f < M_+^a$	
Area decrease	Heat addition
$M_f\uparrow$	$M_f\uparrow$
$\Delta T\uparrow$	$\Delta T\downarrow$

Diverging section					
$M_f < M_+^a$		$M_+ < M_f < 1^a$		$M_f > 1$	
Area increase	Heat addition	Area increase	Heat addition	Area increase	Heat addition
$M_f\downarrow$	$M_f\uparrow$	$M_f\downarrow$	$M_f\uparrow$	$M_f\uparrow$	$M_f\downarrow$
$\Delta T\downarrow$	$\Delta T\downarrow$	$\Delta T\downarrow$	$\Delta T\uparrow$	$\Delta T\uparrow$	$\Delta T\downarrow$

[a]M_+ is given by Eq. (73).

ing the mass flow rate. (Note that in all the previous cases the pressure profile upstream of the throat remains the same.) The usual pressure "hump" due to the condensation shock has disappeared and the pressure decreases monotonically. The frozen Mach number crosses unity somewhere in the diverging section and there is now only one sonic point in the whole field (compared to two in the supercritical case). The variation of subcooling is more interesting in the sense that although the inlet stagnation temperature is substantially lower than the steady supercritical case (in the present example the difference in T_0 between curves c and d is 20 K), the location where the maximum subcooling occurs has not changed significantly. This somewhat surprising result can be explained by the unintuitive laws of compressible fluid dynamics (for example, Table I shows that heat addition decreases vapor temperature if $1 > M_f > M*$). We may construct Table II to explain the variation of Mach number and subcooling in a condensing flow from the information given in Table I.

Thus the heat release adjusts itself such that, in the region $M_+ < M_f < 1$, only a part of the condensation takes place and ΔT still decreases as a result of increasing flow area. The resulting heat release is, however, sufficient to raise the Mach number to unity, which then increases further because of the diverging flow area. [Theoretically, the flow region $M_+ < M_f < 1$ could occur in the converging section if the condensational heat release was practically over before M_f reached M_+. Equations (71) and (72) give the general expressions for the variation of subcooling and frozen Mach number and suggest the possibilities of a quite complex variation depending on the shape of the channel, stagnation conditions, and the properties of the fluid.]

Homogeneous condensation in steam at subsonic velocities requires a subcooled vapor at the nozzle inlet. This is not realizable in a conventional nozzle experiment with the vapor generated in a boiler. Hence this type of wave has not been observed in the usual laboratory experiments and is not reported in the literature. However, in a multistage steam turbine used for electricity generation, steam expands through a series of blade passages and may become subcooled at the inlet of the nucleating stage because of

work extraction in the previous stages. (Reference 33 describes a new theory of nucleation of water droplets in multistage steam turbines.)

C. Flow map for different regimes of condensation

We have mentioned that the occurrence of a particular type of condensation wave depends on the supply conditions, the mechanism of condensation (homogeneous or heterogeneous), and the exact geometry of the nozzle employed. (The rate of heat release and the variation of flow passage area are very delicately balanced especially when condensation takes place close to the nozzle throat.) A practical guide may, however, be obtained from the control volume analysis presented in Sec. V A. Figure 14 plots different regimes of condensation on a Mach number—subcooling plane for pure steam.

The limiting case for subsonic condensation is calculated from Eq. (53), subject to the condition $M_{f1} < 1$, $M_{e2} = 1$ (i.e., downstream equilibrium Mach number is unity). The limiting case of the subcritical condensation shock is calculated from Eq. (53) again, subject to the
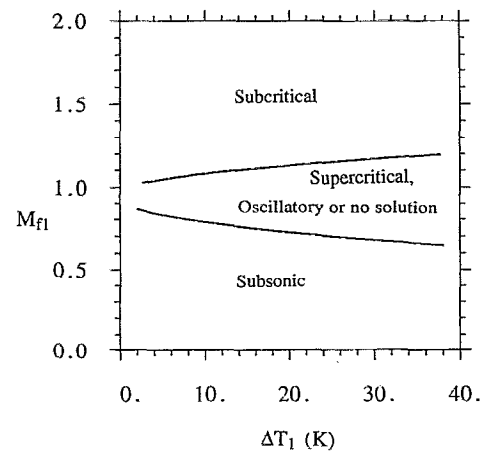

FIG. 14. Flow map for different condensation regimes in low-pressure, pure steam in terms of the frozen Mach number and subcooling at the Wilson point (results from the control volume analysis of Sec. V A).

condition that the downstream *frozen* Mach number is unity ($M_{f2}=1$, $M_{f1}>1$). If a particular combination of subcooling and frozen Mach number at the Wilson point falls above the top line in Fig. 14, one certainly obtains supersonic, subcritical condensation. If the point lies below the bottom line, one obtains subsonic condensation. An operating point within the two limiting lines indicates the possible occurrence of a supercritical condensation wave (with embedded frozen shock), or unsteady flow. *The effect of heat release is very pronounced when the Mach number lies approximately between 0.8 and 1.1, and a small amount of condensation may alter the flow velocity, etc., quite dramatically.*

VI. SUMMARY OF AERODYNAMIC SHOCK WAVES

Depending on the flow conditions, four different types of aerodynamic shock wave structures may be obtained in a gas–vapor-droplet flow.

(i) Equilibrium partly dispersed: The fluid is at two-phase equilibrium both upstream and downstream of the shock wave. There is a frozen shock wave followed by a relaxation zone. This occurs when $M_{f1}>1$ and $y_1>y_{1,\text{lim}}$. Equations (36)–(38) provide approximate jump conditions, while Eq. (40) provides an exact jump condition. The value of $y_{1,\text{lim}}$ is determined from Eq. (41). The form of the approximate equations (36)–(38) is similar to the well-known Rankine–Hugoniot relations for ideal gas and the shock relations are explicitly written in terms of the upstream parameters only.

(ii) Equilibrium fully dispersed: The fluid is at two-phase equilibrium at both ends of the shock wave. However, there is no frozen shock involved. This occurs when $M_{f1}<1$, $M_{e1}>1$, and $y_1>y_{1,\text{lim}}$. Equations (36)–(38) provide approximate jump conditions, while Eq. (40) provides an exact jump condition.

(iii) Partly dispersed with complete evaporation: A frozen shock is involved. The vapor is superheated downstream of the relaxation zone. This occurs when $M_{f1}>1$ and $y_1<y_{1,\text{lim}}$. Equation (47) or the equation set (48) and (49) provide exact jump conditions. Of these, Eq. (47) provides the shock relations in terms of the upstream parameters *only*.

(iv) Fully dispersed with complete evaporation: The vapor is superheated downstream of the dispersed wave but there is no frozen shock. This occurs when $M_{f1}<1$, $M_{e1}>1$ and $y_1<y_{1,\text{lim}}$. Equation (47) or the equation set (48) and (49) provide exact jump conditions.

It should be noted that equations of the form of the classical Rankine–Hugoniot relations [Eqs. (36)–(39) with γ_e replaced by some suitable γ] are *exact* and hold *unconditionally* for ideal gas or even for a two-phase mixture of solid-particle-laden gas. They are only *approximate* and apply *conditionally* in the case of vapor-droplet flows. Interphase mass transfer renders a vapor-droplet medium more difficult to analyze, and complete evaporation through which a two-phase medium turns into a single-phase one must be taken into account. Thus one should be extra careful while borrowing ideas from relaxation gasdynamics and applying them directly to vapor-droplet flow.

VII. SUMMARY OF CONDENSATION DISCONTINUITIES

Four different types of condensation discontinuities may occur: subcritical, supercritical, subsonic, and periodic. The flow conditions for their occurrence are presented as a flow map in Fig. 14. The actual combination of subcooling and frozen Mach number at the Wilson point depends on the stagnation conditions and on the nozzle geometry for homogeneous nucleation, and additionally on the number and size distribution of impurity particles for heterogeneous condensation. The jump conditions *across* subcritical and subsonic condensation zones in a constant area duct, both for homogeneous as well as heterogeneous condensations, are given by Eq. (53), which is exact and explicit. However, Eq. (53) also gives some solutions (the sections between the marks $\times$ and $+$ in Figs. 7–11) where the predicted downstream velocity lies in the range a_e–a_f, where the vapor-droplet mixture cannot be at equilibrium, and hence these solutions are not physically realistic.

VIII. SUMMARY OF THE DIFFERENTIAL ANALYSIS

Isentropic exponents for a gas–vapor-droplet flow under frozen and equilibrium conditions are derived [Eqs. (13) and (24)]. It is shown that although the energy equation for a gas–vapor-droplet mixture can be written in the form of Eq. (35) which is analogous to its single-phase counterpart, it is applicable only under isentropic conditions.

Gasdynamic equations for vapor-droplet flow, including area variation and interphase transport of mass, momentum, and energy, are derived [Eqs. (65)–(72)]. Equations in this full form are to be considered for making correct physical interpretations, e.g., determining the conditions for thermal choking. These equations also indicate to what extent the effect of the interphase transport processes can be modeled by external heat addition to a single-phase fluid [compare Eqs. (65)–(72) with (A1)–(A4)]. The time-marching solution of the gasdynamic equations can predict the proper variation of different flow variables *within* any type of condensation wave in a nozzle (Fig. 12, see also Ref. 5).

ACKNOWLEDGMENT

APPENDIX A: EFFECTS OF EXTERNAL HEAT TRANSFER TO AN IDEAL GAS

If dq is the rate of external heat transfer to the flow of an ideal gas and if A is the flow area, then it is easy to find the rate of change of different flow parameters. The result is

$$\frac{dV}{V}=\frac{1}{1-M^2}\left(-\frac{dA}{A}+\frac{dq}{c_pT}\right), \tag{A1}$$

$$\frac{dp}{p}=\frac{\gamma M^2}{1-M^2}\left(\frac{dA}{A}-\frac{dq}{c_pT}\right), \tag{A2}$$

Phys. Fluids, Vol. 6, No. 5, May 1994

Abhijit Guha   1911

$$\frac{dT}{T} = \frac{1}{1-M^2}\left((\gamma-1)M^2\frac{dA}{A} + (1-\gamma M^2)\frac{dq}{c_pT}\right), \quad \text{(A3)}$$

$$\frac{dM}{M} = \frac{1}{1-M^2}\left[-\left(1+\frac{\gamma-1}{2}M^2\right)\frac{dA}{A}\right.$$

$$\left. +\frac{1}{2}(1+\gamma M^2)\frac{dq}{c_pT}\right]. \quad \text{(A4)}$$

The sign of the rate of change of different flow properties thus depends on the (often competing) effects of area change and heat addition. [The $1-M^2$ terms in the denominator of Eqs. (A1)–(A4) indicate that the flow is sensitive to heat transfer or area change particularly when the Mach number is close to unity.] One may consider a constant-area duct in order to study the effects of heat addition alone. Equation (A2) shows that heat addition results in a rise in pressure in supersonic flow and a decrease in pressure in subsonic flow. Equation (A3) shows that for flow conditions such that $1 > M > 1/\sqrt{\gamma}$, heat addition results in a *decrease* in temperature, which is counterintuitive. Equation (A4) shows that heat addition always drives the flow to sonic conditions. Therefore, there is a maximum quantity of heat, q_{crit}, that the flow can absorb before becoming thermally choked $(M=1)$. It can easily be shown that

$$q_{crit} = \frac{(M^2-1)^2}{2(\gamma+1)M^2\{1+[(\gamma-1)/2]M^2\}}. \quad \text{(A5)}$$

Now, the Mach numbers upstream and downstream of a shock wave are related by

$$M_2^2 = \frac{1+[(\gamma-1)/2]M_1^2}{\gamma M_1^2 - [(\gamma-1)/2]}. \quad \text{(A6)}$$

Substitution of Eq. (A6) in Eq. (A5) shows that

$$q_{crit} = \frac{(M_1^2-1)^2}{2(\gamma+1)M_1^2(1+[(\gamma-1)/2]M_1^2)}$$

$$= \frac{(M_2^2-1)^2}{2(\gamma+1)M_2^2(1+[(\gamma-1)/2]M_2^2)}. \quad \text{(A7)}$$

It can be seen that *a shock wave (across which the total enthalpy h_0 remains constant) does not change the magnitude of the critical quantity of heat in an ideal gas.* This fact can also be appreciated by plotting the Rayleigh line in the (h_0, V) plane.

APPENDIX B: INSTABILITIES OF NONEQUILIBRIUM VARIABLES IN PURE VAPOR-DROPLET FLOW

It is possible to derive the equations for the variation nonequilibrium variables such as ΔV and ΔT_l [similar to Eq. (71) for the variation of ΔT] from the conservation equations given in Sec. V B 1. However, the qualitative behavior may be appreciated by assuming a constant-area duct and that the three relaxation processes take place in three separate stages (which is only approximately true). The justification for this assumption rests on the disparity of the magnitude of the different relaxation times. It has been shown that, in general, for a pure vapor-droplet flow

$\tau_D \ll \tau_1 \ll \tau_T$.[18] (i) The first stage of relaxation: frozen momentum and heat transfer (mathematically, $\tau_I \to \infty$, $\tau_T \to \infty$).

The conservation and interphase equations in a constant-area duct simplify to

$$\frac{d(\Delta T_l)}{dt} + \left(\frac{1-M'^2}{1-M_f^2}\right)\frac{\Delta T_l}{\tau_D} = 0, \quad \text{(B1)}$$

where $M' = V_v/a'$, V_v is the vapor velocity and the intermediate sound speed a' is given by

$$a'^2/a_f^2 = \{1+[y/(1-y)](\gamma_v c_l/R_v)(R_v T_s/h_{fg})^2\}^{-1}. \quad \text{(B2)}$$

Usually a' is very close to a_f. Equation (B1) shows that ΔT_l shows instability (i.e., any perturbation in $|\Delta T_l|$ grows and takes the system further away from equilibrium) when the flow velocity lies in the range $a' < V_v < a_f$. (ii) The second stage: equilibrium droplet temperature and frozen heat transfer [mathematically, $\Delta T_l/\tau_D \to V_l(dT_s/dx)$, $\tau_T \to \infty$].

The conservation and interphase equations in a constant-area duct simplify to

$$\frac{d(\Delta V)}{dt} + \left(\frac{1-M''^2}{1-M'^2}\right)\frac{\Delta V}{\tau_I} = 0, \quad \text{(B3)}$$

where $M'' = V_v/a''$ and the intermediate sound speed a'' is given by

$$a''^2/a_f^2 = (1-y)\{1+[y/(1-y)](\gamma_v c_l/R_v)$$

$$\times (R_v T_s/h_{fg})^2\}^{-1} \quad \text{(B4)}$$

or

$$a''^2 = (1-y)a'^2. \quad \text{(B5)}$$

Equation (B3) shows that ΔV shows instability when the flow velocity lies in the range $a'' < V_v < a'$. (iii) The third stage: equilibrium droplet temperature and momentum transfer [mathematically, $\Delta T_l/\tau_D \to (dT_s/dt)$, $\Delta V/\tau_I \to (dV_v/dt)$].

The conservation and interphase equations in a constant-area duct simplify to

$$\frac{d(\Delta T)}{dt} + \left(\frac{1-M_e^2}{1-M''^2}\right)\frac{\Delta T}{\tau_T} = 0, \quad \text{(B6)}$$

where $M_e = V_v/a_e$ and a_e is the equilibrium speed of sound.

Equation (B6) shows that ΔT shows instability when the flow velocity lies in the range $a_e < V_v < a''$. All this
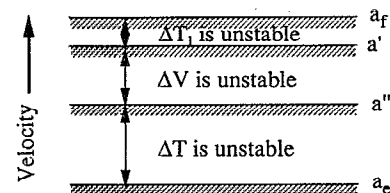
FIG. 15. Instability of nonequilibrium variables in pure vapor-droplet flow.

Abhijit Guha

behavior has been schematically shown in Fig. 15. (Similar behavior would be observed when a carrier gas is present as well.) The relationship of the four sound speeds to each other is of great importance. As a typical example, for steam at 1 bar pressure and wetness fraction 0.1

$$a_f : a' : a'' : a_e \equiv 1:0.997:0.945:0.878.$$

[1] P. G. Hill, "Condensation of water vapor during supersonic expansion in nozzles," J. Fluid Mech. **25**, 593 (1966).

[2] G. Gyarmathy, in *Two-phase Steam Flow in Turbines and Separators*, edited by M. J. Moore and C. H. Sieverding (Hemisphere, Washington, 1976), Chap. 3.

[3] P. P. Wegener, "Gasdynamics of expansion flows with condensation, and homogeneous nucleation of water vapor," in *Nonequilibrium Flows*, edited by P. P. Wegener (Marcel Dekker, New York, 1969), Part I, Chap. 4.

[4] P. P. Wegener and D. J. Cagliostro, "Periodic nozzle flow with heat addition," Combust. Sci. Technol. **6**, 269 (1973).

[5] A. Guha and J. B. Young, "Time-marching prediction of unsteady condensation phenomena due to supercritical heat addition," Proceedings of the Conference on Turbomachinery: Latest developments in a Changing Scene, London, IMechE Paper C423/057, 1991, pp. 167–177.

[6] D. Barschdorff and G. A. Fillipov, "Analysis of certain special operating modes of laval nozzles with local heat supply," Heat Transfer—Sov. Res. **2**, 76 (1970).

[7] A. A. Pouring, "Thermal choking and condensation in nozzles," Phys. Fluids **8**, 1802 (1965).

[8] C. A. Moses and G. D. Stein, "On the growth of steam droplets formed in a laval nozzle using both static pressure and light scattering measurements," J. Fluids Eng. ASME **100**, 311 (1978).

[9] J. P. Sislian and I. I. Glass, "Condensation of water vapor in rarefraction waves: I. Homogeneous nucleation," AIAA J. **14**, 1731 (1976).

[10] G. Schnerr and U. Dohrmann, "Theoretical and experimental investigation of 2-D diabatic transonic and supersonic flow fields," *Proceedings IUTAM—Symposium Transsonicum III*, edited by J. Zierep and H. Oertel (Springer, New York, 1988), pp. 125–135.

[11] H. J. Smolders, E. M. J. Niessen, and M. E. H. van Dongen, "On the similarity character of an unsteady rarefraction wave in a gas-vapor mixture with condensation," in *Adiabatic Waves in Liquid–Vapor Systems*, edited by G. E. A. Meier and P. A. Thompson (Springer, New York, 1989), pp. 197–205.

[12] F. E. Marble, "Some gasdynamic problems in the flow of condensing vapors," Astronaut. Acta **14**, 585 (1969).

[13] R. Jackson and B. J. Davidson, "An equation set for nonequilibrium two-phase flow, and an analysis of some aspects of choking, acoustic propagation, and losses in low-pressure wet steam," Int. J. Multiphase Flow **9**, 491 (1983).

[14] E. Becker and G. Bohme, in *Nonequilibrium Flows*, edited by P. P. Wegener (Marcel Dekker, New York, 1969), Part I, Chap. 2.

[15] G. Rudinger, "Some properties of shock relaxation in gas flows carrying small particles," Phys. Fluids **7**, 658 (1964).

[16] A. Guha, "Jump conditions across normal shock waves in pure vapor-droplet flows," J. Fluid Mech. **241**, 349 (1992).

[17] A. Guha, "Structure of partly dispersed normal shock waves in vapor-droplet flows," Phys. Fluids A **4**, 1566 (1992).

[18] A. Guha, "The physics of relaxation processes and of stationary and nonstationary shock waves in vapor-droplet flows," in *Transport Phenomena in Heat and Mass Transfer*, ISTP IV, edited by J. Reizes (Elsevier, New York, 1992), pp. 1404–1417.

[19] J. B. Young and A. Guha, "Normal shock-wave structure in two-phase vapor-droplet flows," J. Fluid Mech. **228**, 243 (1991).

[20] A. Guha and J. B. Young, "Stationary and moving normal shock waves in wet steam," in *Adiabatic Waves in Liquid–Vapor Systems*, edited by G. E. A. Meier and P. A. Thompson (Springer, New York, 1989), pp. 159–170.

[21] A. Konorski, "Shock waves in wet steam flow," PIMP **57**, 101 (1971).

[22] V. Petr, "Nonlinear wave phenomena in wet steam," Eighth Conference on Steam Turbines of Large Output, Plsen, 1979, pp. 248–265.

[23] H. W. J. Goossens, J. W. Cleijne, H. J. Smolders, and M. E. H. van Dongen, "Shock wave induced evaporation of water droplets in a gas-droplet mixture," Exp. Fluids **6**, 561 (1988).

[24] E. Becker, "Relaxation effects in gasdynamics," Aeronaut. J. **74**, 736 (1970).

[25] J. P. Sislian, "Condensation of water vapor with or without a carrier gas," Report No. 201, Institute for Aerospace Studies, University of Toronto, 1975.

[26] L. D. Landau and E. M. Lifshitz, *Fluid Mechanics*, 2nd ed. (Pergamon, New York, 1989), Chap. 15.

[27] J. B. Young, "Condensation in jet engine intake ducts during stationary operation," ASME Paper 93-GT-5, 1993.

[28] S. A. Skillings, M. J. Moore, P. T. Walters, and R. Jackson, "A reconsideration of wetness loss in LP steam turbines," BNES conference on Technology of Turbine Plant Operating with Wet Steam, London, 1988 pp. 147–153.

[29] P. A. Blythe and C. J. Shih, "Condensation shocks in nozzle flows," J. Fluid Mech. **76**, 593 (1976).

[30] J. H. Clarke and C. F. Delale, "Nozzle flows with nonequilibrium condensation," Phys. Fluids **29**, 1398 (1986).

[31] P. P. Wegener and L. M. Mack, "Condensation in supersonic and hypersonic wind tunnels," in *Advances in Applied Mechanics* (Academic, New York, 1958), Vol. V, pp. 307–447.

[32] J. D. Denton, "An improved time-marching method for turbomachinery flow calculation," Trans. A.S.M.E. (J. Eng. Power), **105**, 514 (1983).

[33] A. Guha and J. B. Young, "The effects of flow unsteadiness on the homogeneous nucleation of water droplets in steam turbines," to appear in Philos. Trans. R. Soc. Ser. A.

[34] S. A. Skillings, P. T. Walters, and M. J. Moore, "A study of supercritical heat addition as a potential loss mechanism in condensing steam turbines," IMechE Conference, Cambridge, England, Paper C259/87, 1987, pp. 125–134.

[35] A. Guha, "Thermal choking due to nonequilibrium condensation," to appear in ASME J. Fluids Eng.

Phys. Fluids, Vol. 6, No. 5, May 1994

Abhijit Guha   1913